THE JOURNAL OF BIOLOGICAL CHEMISTRY VOL. 291, NO. 43, pp. 22721–22740, October 21, 2016

The C Terminus of the RNA Polymerase II Transcription Factor IID (TFIID) Subunit Taf2 Mediates Stable Association of Subunit Taf14 into the Yeast TFIID Complex*[S]

Received for publication, July 29, 2016, and in revised form, August 31, 2016 Published, JBC Papers in Press, September 1, 2016, DOI 10.1074/jbc.M116.751107

Jordan T. Feigerle[1] **and P. Anthony Weil**[2]

From the Department of Molecular Physiology and Biophysics, Vanderbilt University School of Medicine, Nashville, Tennessee 37232-0615

The evolutionarily conserved RNA polymerase II transcription factor D (TFIID) complex is composed of TATA box-binding protein (TBP) and 13 TBP-associated factors (Tafs). The mechanisms by which many Taf subunits contribute to the essential function of TFIID are only poorly understood. To address this gap in knowledge, we present the results of a molecular genetic dissection of the TFIID subunit Taf2. Through systematic site-directed mutagenesis, we have discovered 12 *taf2* temperature-sensitive (*ts*) alleles. Two of these alleles display growth defects that can be strongly suppressed by overexpression of the yeast-specific TFIID subunit *TAF14* but not by overexpression of any other TFIID subunit. In *Saccharomyces cerevisiae*, Taf14 is also a constituent of six other transcription-related complexes, making interpretation of its role in each of these complexes difficult. Although Taf14 is not conserved as a TFIID subunit in metazoans, it is conserved through its chromatin-binding YEATS domain. Based on the Taf2-Taf14 genetic interaction, we demonstrate that Taf2 and Taf14 directly interact and mapped the Taf2-Taf14 interaction domains. We used this information to identify a Taf2 separation-of-function variant (Taf2-ΔC). Although Taf2-ΔC no longer interacts with Taf14 *in vivo* or *in vitro*, it stably incorporates into the TFIID complex. In addition, purified Taf2-ΔC mutant TFIID is devoid of Taf14, making this variant a powerful reagent for determining the role of Taf14 in TFIID function. Furthermore, we characterized the mechanism through which Taf14 suppresses *taf2*^{ts} alleles, shedding light on how Taf2-Taf14 interaction contributes to TFIID complex organization and identifying a potential role for Taf14 in mediating TFIID-chromatin interactions.

RNA polymerase II and the general RNA polymerase II transcription factors (TFIIA,[3] -B, -D, -E, -F, and -H) are required for mRNA gene transcription in all eukaryotes (1, 2). These factors assemble at gene promoters to form the preinitiation complex (PIC), a macromolecular assembly required for accurate initiation of transcription. A rate-limiting step for PIC formation is the association of TBP, or its multisubunit chaperones TFIID and SAGA, with the promoter. In the yeast *Saccharomyces cerevisiae* (Sc), SAGA dominates on gene promoters that respond to stress, whereas TFIID dominates on so-called "housekeeping" genes (3–5). These housekeeping genes often do not contain consensus TATA boxes (so-called "TATA-less" genes, although these genes do contain TATA-like sequences) and instead probably rely on the ability of TFIID to engage with promoter DNA and/or active chromatin to stimulate transcription (6, 7).

The evolutionarily conserved TFIID complex is composed of TBP and 13 TBP-associated factors (Tafs 1–13) (8, 9). Tafs display myriad biochemical activities including binding to promoter-DNA (10–19), binding to or enzymatically modifying chromatin (20–25), binding to gene-specific transactivators (26–29), binding to the general transcription factors (30–34), and binding to Mediator (35). However, few examples exist where the importance of these activities has been genetically and biochemically interrogated to assess the impact of loss-of-function variants on transcription activation (25, 30, 31, 36, 37).

The overall trilobed structure of TFIID is conserved between budding yeast and metazoans (38, 39). In addition, our laboratory has defined the subunit stoichiometry and location of the evolutionarily conserved TFIID subunits using electron microscopy (EM) coupled with difference mapping and immunolabeling (8, 40–42). Consistent with these findings, a reconstituted human eight-Taf complex (Tafs 2, 4, 5, 6, 8, 9, 10, and 12) docks well into the yeast TFIID structure and displays subunit stoichiometry similar to yeast TFIID (43, 44).

* This work was supported in part by National Institutes of Health Grant R01 GM115892 (to P. A. W.) and National Institutes of Health Center Core Grant 5P30CA068485-18. The authors declare that they have no conflicts of interest with the contents of this article. The content is solely the responsibility of the authors and does not necessarily represent the official views of the National Institutes of Health.

[S] This article contains supplemental Tables 1 and 2.

[1] Supported by National Institutes of Health Grant T32 GM008554.

[2] To whom correspondence should be addressed: Dept. of Molecular Physiology and Biophysics, Vanderbilt University School of Medicine, Nashville, TN 37232-0615. Tel.: 615-322-7007; Fax: 615-322-7236; E-mail: tony.weil@vanderbilt.edu.

[3] The abbreviations used are: TFIIA (-B, -D, -E, -F, -H), RNA polymerase II transcription factor A (-B, -D, -E, -F, -H); TBP, TATA box-binding protein; Taf, TBP-associated factor; Ts, temperature-sensitive; YEATS, Yaf9, Enl, Af9, Taf14, Sas5; PIC, preinitiation complex; SAGA, Spt-Ada-Gcn5-acetyltransferase; INR, initiator; H3K9, lysine 9 of histone H3; ScTFIID, *S. cerevisiae* TFIID; I-TASSER, Iterative Threading Assembly Refinement; MBP, maltose-binding protein; TAP, tandem affinity purification; Ni^{2+}-NTA, nickel-nitrilotriacetic acid; SWI/SNF, switching-deficient/sucrose non-fermenting complex; RSC, remodel the structure of chromatin complex; RPG, ribosomal protein-encoding gene; PHD, plant homeobox domain; 5-FOA, 5-fluoroorotic acid; SC, synthetic complete medium; YPD, yeast extract, peptone, dextrose; qRT-PCR, quantitative reverse transcription-PCR; IP, immunoprecipitation; BA, buffer A; aa, amino acid(s); NLS, nuclear localization sequence; Pol, polymerase; Bis-Tris, 2-[bis(2-hydroxyethyl)amino]-2-(hydroxymethyl)propane-1,3-diol.

Budding yeast does display some significant differences with regard to TFIID structure and promoter architecture. First, the metazoan Taf1 double bromodomain and the Taf3 plant homeobox domain (PHD) finger, domains that directly interact with modified chromatin, are missing from the yeast homologs (45–47). Second, yeast TFIID contains an additional subunit, Taf14 (8). Third, in metazoan TFIID, Tafs 1 and 2 bind to the initiator (INR) core promoter element (10, 12), and Tafs 6 and 9 bind to the downstream promoter element (11). Neither the INR nor the downstream promoter element has been unambiguously identified in the yeast system (1).

Despite these differences, yeast have evolved mechanisms to achieve similar TFIID promoter-DNA binding and chromatin recognition activities. Instead of having a double bromodomain covalently attached to Taf1, the double bromodomain protein Bdf1 (bromodomain factor-1) is a TFIID-associated protein (48, 49), and its occupancy in genome-wide analyses correlates with Taf1 occupancy (7). Although not conserved as a TFIID subunit, Taf14 is conserved through its YEATS domain (50). This domain, which is also present in the super elongation complex proteins AF-9 and ENL (51–53), was recently shown to bind to acetylated and crotonylated lysine 9 of histone H3 (H3K9) (23, 24), marks associated with active transcription (54, 55). In regard to ScTFIID promoter recognition, footprinting analyses have demonstrated that both metazoan and ScTFIID display extended footprints with contacts spanning nearly 100 bp (8, 17, 56). ScTFIID histone fold pairs Taf4/Taf12 and Taf6/Taf9 also display *in vitro* DNA binding activities, although binding has not been shown to be sequence-specific (15). In addition, structural analyses with ScTFIID-TFIIA-activator in complex with promoter-DNA position DNA in contact with the C terminus of Taf2 (57). Taken together, these observations demonstrate that TFIID promoter-DNA and chromatin interaction activities are maintained in the yeast system. However, how these activities contribute to TFIID transcriptional activation function remains undefined.

In addition to its role in TFIID, Taf14 is also a subunit or associated protein of six other transcription-related complexes (52, 58–60). Although Tafs 1–13 are essential for life (46, 61–65), Taf14-null cells display temperature-sensitive (Ts) growth and defects in expression of galactose (*GAL*) and DNA repair genes (23, 52). Still, how Taf14 contributes to TFIID structure or function remains poorly understood because mutations in *TAF14* could impact the function of all of the transcription-related complexes with which it associates. To begin to understand *TAF14* function *in vivo*, we need true separation-of-function variants that can specifically dissociate Taf14 from a single complex without disrupting its ability to perform its other functions.

We have minimal understanding of Taf2 function despite the fact that it was the first yeast Taf discovered (10, 46, 61). Our laboratory was the first to discover the location of Taf2 within the TFIID complex (41). In addition to its INR binding function, metazoan Taf2 directly interacts with Taf8, and this interaction is critical for Taf2 to localize to the nucleus (44). For RNA polymerase II to clear the promoter and begin productive elongation, TFIID appears to isomerize in a Taf2-dependent manner to release TFIID from downstream promoter sequences (66, 67). However, none of these biochemical activities have been genetically dissected. In fact, Taf2 has never been subjected to structure-function analysis in any system. While this manuscript was in preparation, a cryo-EM structure of human TFIID allowed Louder *et al.* (68) to describe the structure of Taf2 in molecular detail. However, this structure was not interrogated genetically or biochemically. Consequently, we have minimal understanding of how Taf2 contributes to TFIID-dependent transcription *in vivo*.

In this study, we performed a systematic molecular genetic dissection of Taf2 to address this gap in knowledge. Our analyses identified a genetic interaction between *TAF2* and *TAF14*. We demonstrate that these two subunits directly interact and define the interaction domains in both subunits. Despite Taf14 being present in multiple copies per TFIID subunit, mutation in Taf2 can completely disrupt the ability of Taf14 to associate with the TFIID complex. Taf14-less TFIID-containing cells display defects in growth and transcript abundance for the highly transcribed TFIID-dominated ribosomal protein-encoding genes. Furthermore, our data indicate that the Taf14 YEATS domain contributes to TFIID function.

Results

I-TASSER Prediction of Taf2 Structures—To understand the role of Taf2 in TFIID function, we initially pursued classical approaches that have been successfully used to identify TFIID subunit functional domains. First, primary amino acid sequences from *S. cerevisiae* (yeast), *Homo sapiens* (human), and *Drosophila melanogaster* (fly) Taf2 were subjected to ClustalW sequence alignment to identify "hot spots" of amino acid sequence homology that we could target for mutagenesis. These analyses have been successfully applied to the histone fold domain-containing Tafs as well as the conserved TBP C terminus (47, 62, 63, 65, 69). Yeast Taf2, which encodes a 1407-aa protein, only displays weak sequence conservation with human (1199 aa) and fly (1221 aa) Taf2, ~15% sequence identity and ~32% sequence similarity (Fig. 1, *B* and *C*). In addition, the amino acids that are conserved do not cluster in hot spots but instead are distributed throughout the amino acid sequence. Second, we performed systematic ~100-amino acid N-terminal, C-terminal, and internal deletion mutagenesis as described previously (28, 36, 70, 71) to generate 49 deletion variants. *TAF2* is a single copy essential gene. Thus, to perform genetic complementation assays, we used a pseudodiploid *TAF2* wild-type (WT) strain for plasmid shuffle analysis as described previously (28, 32, 36, 47). Forty-eight of these variants were unable to complement a *taf2*-null strain and failed to stably incorporate into the TFIID complex (summarized in supplemental Table 1). The single variant that could complement a *taf2*-null strain (Taf2(1–1307)) displayed no discernible adverse growth, steady-state protein levels, or TFIID stable incorporation phenotypes. Third, we created a hydroxylamine-mutagenized *TAF2* plasmid mutant library (62) to generate $taf2^{ts}$ variants. However, none of the 20 $taf2^{ts}$ alleles identified in a plate growth-based screen displayed acute loss of function in liquid culture when shifted to the non-permissive temperature (37 °C) (data not shown) as has been shown to occur for Ts alleles for every essential yeast Taf (4).

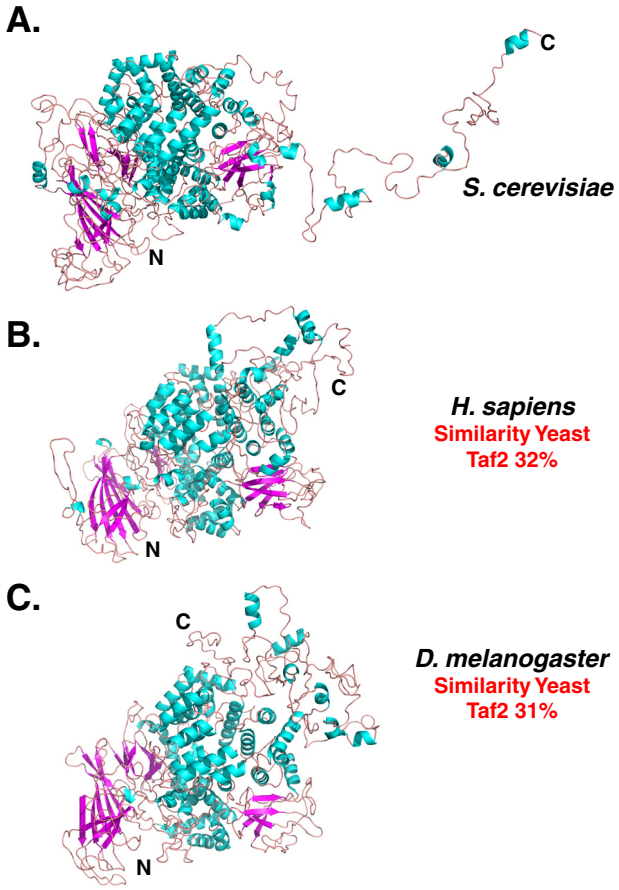

FIGURE 1. **3D structural prediction of Taf2 homologs suggests similar structures despite low overall sequence conservation.** *A–C*, the primary amino acid sequences of *S. cerevisiae* Taf2 (*A*), *H. sapiens* Taf2 (*B*), and *D. melanogaster* Taf2 (*C*) were analyzed using the ClustalW sequence alignment algorithm and the 3D structural prediction program I-TASSER. Evolutionary sequence conservation and predicted 3D structural models indicating secondary structure (*pink*, β-strand; *cyan*, α-helix; *tan*, random coil) are shown. N and C termini are labeled. Sequence alignment similarity scores of *H. sapiens* and *D. melanogaster* compared with *S. cerevisiae* are displayed next to the predicted structures in *B* and *C*, respectively.

To overcome these technical hurdles, we hypothesized that a structure-guided site-directed mutagenesis strategy would successfully identify Taf2 amino acids critical for Taf2 function. However, at the time of this study, no 3D structural information existed for Taf2. Thus, to generate a putative 3D model for Taf2, we used the 3D structural prediction program I-TASSER to generate models for yeast, human, and *Drosophila* Taf2 structures (Fig. 1, *A*, *B*, and *C*, respectively) (72). I-TASSER has been successfully used in the gene regulation field to model structurally intractable proteins (68, 73, 74). Despite the weak amino acid sequence conservation, I-TASSER predicts that the Taf2 structures from these three different organisms display the same general features. Particularly, the N terminus of Taf2 is predicted to contain a β-sheet motif, the central portion and majority of the molecule are composed of HEAT repeats, and the C terminus is predicted to form another β-sheet motif along with an unstructured region. As noted above, while this manuscript was in preparation, a high resolution cryo-EM structure of human Taf2 was described, and it exhibits the same general architecture predicted by our study (68). Given the similarities among the yeast, human, and *Drosophila* Taf2 predicted structures, we concluded that our *in silico* generated yeast Taf2 structure was a suitable model from which to design a structure-based site-directed mutagenesis screen.

Site-directed Mutagenesis of TAF2—To further genetically interrogate yeast *TAF2*, we designed two classes of *TAF2* site-directed variants comprising 87 mutants. These variants primarily consisted of Ala block substitution mutations but also included charge reversal mutations (see supplemental Table 2). Class I mutants, designed based on predicted solvent accessibility and proximity to evolutionarily conserved residues, contained 58 variants. Class II mutants, designed based on predicted solvent inaccessibility and to include mutations of groups of conserved amino acids, contained 29 variants. All variants were engineered to contain a three-copy HA tag and SV40 nuclear localization sequence (HA_{x3}NLS) (HA) N-terminal tag. Importantly, HA-Taf2 phenocopies untagged Taf2 in genetic complementation assays and can efficiently and stably incorporate into the TFIID complex (Fig. 2, *A* and *B*). Every variant was scored for its ability to genetically complement a *taf2*-null strain at both permissive (25 °C) and non-permissive temperatures (37 °C) as well as by α-HA immunoblotting to ensure each variant accumulated to levels similar to WT Taf2.

Results for these analyses are described in detail in supplemental Table 2. In summary, of the Class I variants, 36% displayed a genetic complementation defect including five that were inviable and eight variants that were both slow growing at the permissive temperature and Ts at the non-permissive temperature (Fig. 2; *taf2-ts1* through *taf2-ts8*). Of the Class II variants, 62% displayed a genetic complementation defect including 10 that were inviable and four variants that were both slow growing at the permissive temperature and Ts at the non-permissive temperature (Fig. 2; *taf2-ts9* through *taf2-ts12*). Of note, none of the variants displayed dominant negative phenotypes. Surprisingly, none of the variants displayed drastic reduction in steady-state protein levels (>2×), even variants that could not complement the *taf2*-null strain.

To assess the mechanism by which the loss-of-function Taf2 variants fail to complement the *taf2*-null strain, inviable and $taf2^{ts}$ variants were subjected to α-HA co-immunoprecipitation (co-IP) (Fig. 2*B* and supplemental Table 2). A strain expressing untagged WT Taf2 was used as a negative control. Despite similar steady-state protein levels and IP efficiency, none of the loss-of-function *taf2* mutant variants tested could co-precipitate either the TFIID-specific subunits Taf7 and Taf8 or Taf14 as efficiently as HA-Taf2. These results suggest that these mutations disrupt Taf2-TFIID subunit interactions, contributing to growth defects.

TAF14 Overexpression Suppresses Select $taf2^{ts}$ Growth Phenotypes—Considering that all of the loss-of-function *taf2* variants display defects in stable incorporation into the TFIID complex, likely as a result of disruption of specific Taf2-TFIID subunit interactions, we hypothesized that artificially driving Taf2-TFIID stable incorporation would suppress the $taf2^{ts}$-associated growth defects. Ideally, if a $taf2^{ts}$ mutant variant has a reduction in binding affinity to a TFIID subunit, increasing concentration of that subunit could drive complex formation and rescue the ability of Taf2 to stably associate with TFIID. To this end, we individually overexpressed every TFIID subunit

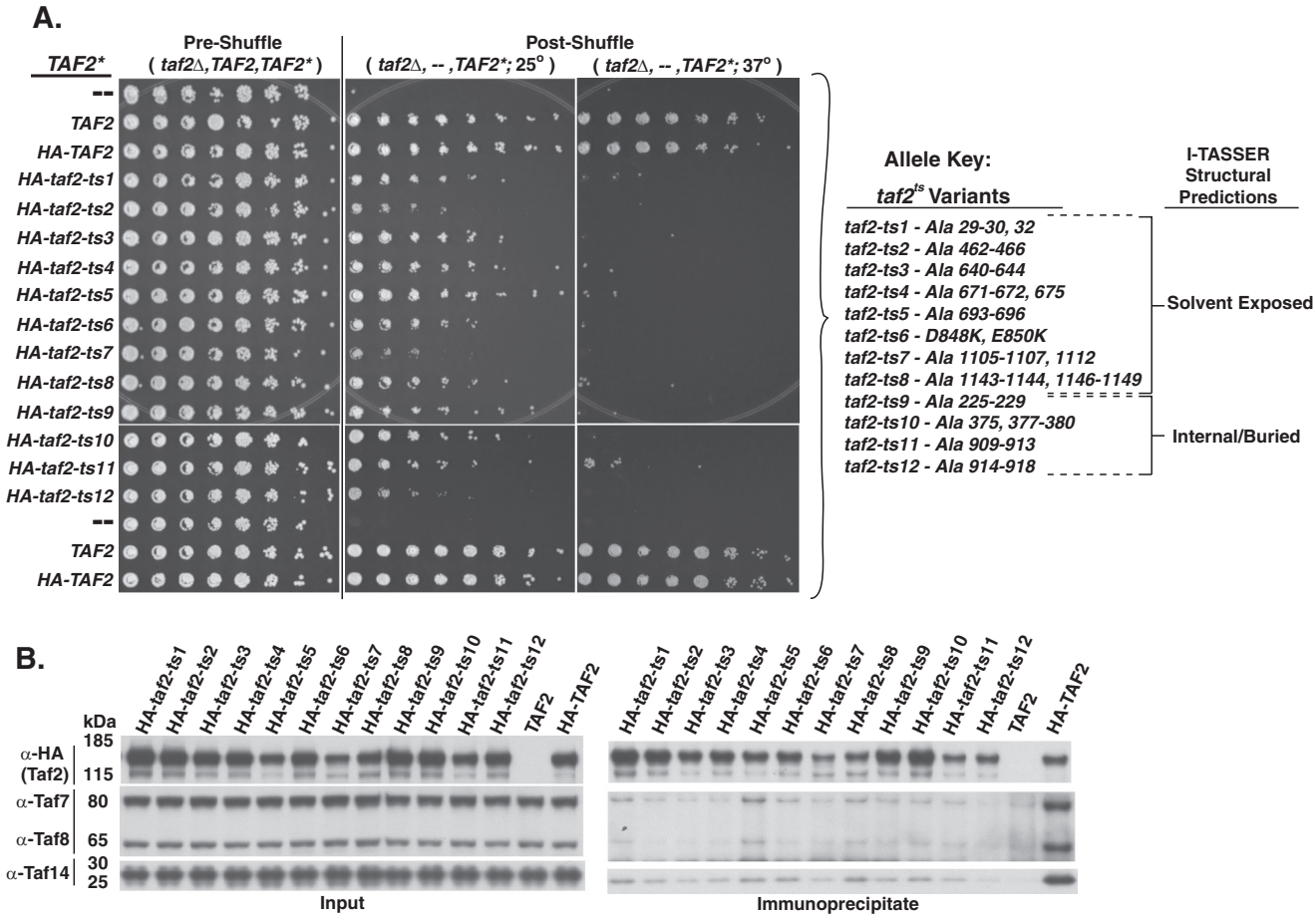

FIGURE 2. **Identification of *taf2ts* alleles using structural prediction and amino acid conservation-guided site-directed mutagenesis.** *A*, genetic complementation assay. *taf2*-null cells harboring both *URA3*-marked *TAF2* and *LEU2*-marked *TAF2** plasmids were serially diluted 1:4 from *left* to *right* and spotted with a pinning tool onto either SC −Leu (*Pre-Shuffle*) or SC −Leu + 5-FOA to select for cells that have spontaneously lost the *URA3*-marked *TAF2* plasmid (*Post-Shuffle*). Plates were grown for 72 h at 37 °C or 96 h at 25 °C prior to imaging. *TAF2**, test gene (either no ORF (−), *TAF2*, HA_{x3}*NLS-TAF2*, or various HA_{x3}*NLS*-tagged *taf2* Ts alleles (HA_{x3}*NLS-taf2-ts1* through *-ts12*)). The variant amino acids in the *taf2ts* alleles are shown in the *Allele Key* to the *right* (*taf2ts* variants). Representative plate images from at least two biological replicates are presented. HA_{x3}NLS tag is labeled as HA in all figures. *B*, Taf2-TFIID co-IP. Whole cell extracts derived from the strains containing TAF2* (*TAF2*, HA_{x3}*NLS-TAF2*, and *-taf2-ts1* through *-ts12*) described in *A* were used for immunoprecipitation with the anti-HA mAb 12CA5 IgG. One percent of the lysate (*Input*) and 33% of the pellet (*Immunoprecipitate*) were separated via SDS-PAGE, blotted to PVDF membrane, and probed with anti-HA (α-HA(Taf2)) and the indicated anti-Taf IgGs (α-Taf7, α-Taf8, and α-Taf14). Representative immunoblots from at least two biological replicates are presented.

(Fig. 3*A*) in strains harboring the *taf2ts* variants. We have previously shown that overexpressed TFIID subunits *TAF4* and *TAF11* have displayed positive genetic interactions with *TOA2*, a protein that directly interacts with the TFIID complex, demonstrating that overexpression of individual TFIID subunits is a viable method for identifying genetic interactions (32).

Overexpression of *TAF1*, *TAF3*, *TAF7*, *TAF8*, and *TAF14* resulted in dominant negative growth phenotypes, consistent with published results (75). As expected, overexpression of *TAF2* could complement growth for all *taf2ts* variants (Fig. 3*B* and data not shown). In addition, we observed strong *taf2ts* allele-specific suppression when we overexpressed *TAF14* but not for any of the other non-*TAF2* TFIID subunits (Fig. 3, *B* and *C*, see *taf2-ts6 versus taf2-ts7* and *ts8*). *TAF14* overexpression suppression of the *taf2-ts7*-associated growth phenotype was particularly potent, rescuing growth to near WT levels at both permissive and non-permissive temperatures.

Although five of the 12 *taf2ts* variants displayed mild growth improvement, *TAF14* overexpression suppression of *taf2-ts7* and *-ts8* significantly improved growth at all temperatures tested. The amino acids mutated in the *taf2-ts7* and *-ts8* variants map to adjacent α-helixes in the yeast Taf2 predicted structure, whereas *taf2-ts6* is predicted to reside on the opposite side of the molecule (Fig. 3*D*). These results suggest that amino acids mutated in the *taf2-ts7* and *-ts8* form a domain that is likely involved in Taf2-TFIID subunit physical interactions, potentially Taf2-Taf14 interaction. Because of the potency of the genetic interaction between *TAF14* and *taf2-ts7*, further molecular and genetic analyses were performed with *taf2-ts7*.

TAF14 Overexpression Suppresses Defects in Ribosomal Protein Gene Transcript Abundance Associated with taf2-ts7—We hypothesized that strong *taf2-ts7* growth defects likely result in a reduction in abundance of ribosomal protein-encoding gene (RPG) transcripts, a class of genes that is TFIID-dominated (3–7). To assess RPG transcripts, log phase growing yeast strains, harboring either *TAF2* or *taf2-ts7* and containing either an empty overexpression vector or a *TAF14* overexpression vector, were abruptly shifted to the non-permissive temperature for 2 h followed by RNA extraction and quantitative reverse transcription-PCR (qRT-PCR). We have assessed RPG

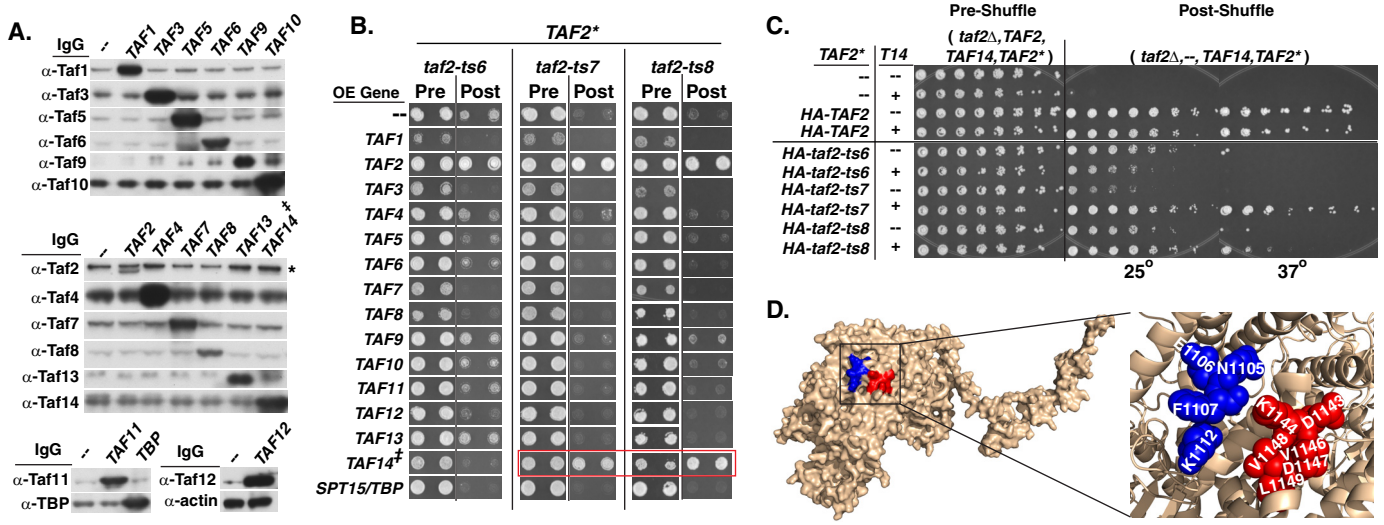

FIGURE 3. **Overexpression of *TAF14* suppresses the slow and Ts growth phenotypes associated with select *taf2*^{ts} mutant variants.** *A*, overexpression of all TFIID subunits in yeast. Whole cell extracts derived from *S. cerevisiae* strains harboring TFIID subunit overexpression (*OE*) plasmids (no ORF (−), Taf1–Taf14, and TBP as indicated) were separated via SDS-PAGE and immunoblotted using anti-TFIID subunit-specific IgGs (α-Taf1 to α-Taf14 and α-TBP) or anti-actin IgG as a loading control for the α-TAF12 blot. *, nonspecific band. ‡ denotes the fact that the cDNA for *TAF14* was used because *TAF14* contains an intron. The image is derived from one replicate. *B*, overexpression suppression of select *taf2*^{ts} mutant strains. Two biological replicates of *taf2*-null cells harboring a *URA3*-marked *TAF2* plasmid, a *LEU2*-marked *TAF2** plasmid (HA_{x3}*NLS-taf2-ts6*, HA_{x3}*NLS-taf2-ts7*, and HA_{x3}*NLS-taf2-ts8*) and a *HIS3*-marked TFIID overexpression plasmid (same TFIID subunits as in *A*) were spotted on SC −Leu,−His medium (*Pre-Shuffle*) or SC −Leu,−His + 5-FOA medium (*Post-Shuffle*) and grown for 72 h at 30 °C for *taf2-ts6* and *taf2-ts7* and 34 °C for *taf2-ts8*. Qualitatively improved growth in both biological replicates beyond the no-ORF control is indicated with a *red box*. *C*, *TAF14* overexpression suppression of *taf2*^{ts} alleles. Plasmid shuffle was performed as in *B* except the *HIS3*-linked overexpression plasmid contains a $FLAG_{x2}$NLS-tagged *TAF14* cDNA and cells were serially diluted 1:4 from *left* to *right* prior to plating. Plates were grown at 25 °C for 96 h or at 37 °C for 72 h prior to imaging (*TAF2**: no ORF (−), HA_{x3}*NLS-TAF2*, HA_{x3}*NLS-taf2-ts6*, HA_{x3}*NLS-taf2-ts7*, and HA_{x3}*NLS-taf2-ts8*). *D*, a surface rendering of the Taf2 I-TASSER-predicted structure (*tan*) highlighting the position of the amino acids mutated in *taf2-ts7* (*blue*) and *taf2-ts8* (*red*). Note that amino acids mutated in *taf2-ts6* are located on the reverse side of the Taf2 predicted structure and hence not visible in this image. In the *blown-up* image, identities of the amino acids mutated in *taf2-ts7* and *taf2-ts8* are in *spheres* with surrounding secondary structure represented by *ribbons*.

transcript abundance using this temperature shift paradigm using Ts variants for *TAF1–TAF13*, *TOA1*, and *TOA2* (28, 32, 36).

We found that *taf2-ts7* without *TAF14* overexpression displays a statistically significant ~3-fold reduction compared with *TAF2* in TFIID-dominated RPG transcripts (*RPS3*, *RPS5*, *RPS8A*, and *RPS9B*; Fig. 4*A*) without a concomitant significant decrease in SAGA-dominated transcripts (*PGK1* and *PYK1*; Fig. 4*A*), RNA polymerase I transcripts (*RDN58*; Fig. 4*B*), or RNA polymerase III transcripts (*SNR6*; Fig. 4*C*) (54). The RPG transcript defects were ameliorated when *TAF14* was overexpressed in the *taf2-ts7* strain. These data suggest that the ability of *taf2-ts7* to appropriately regulate RPG transcript abundance is aided by elevated *TAF14* levels.

TAF2 and TAF14 Directly Interact in Vitro—The simplest model for the genetic interaction between Taf2 and Taf14 is that these two proteins directly interact. Consistent with this hypothesis, Taf2 was identified as a Taf14-interacting protein in a genome-wide yeast two-hybrid screen but was not authenticated as a direct interaction (59). To determine whether Taf2 and Taf14 directly interact, Taf1-TAP-purified TFIID, maltose-binding protein (MBP), and MBP-Taf2, all purified from yeast (see "Materials and Methods"), were subjected to Far-Western blotting with and without purified recombinant His_6-Taf14 (Fig. 5*A*). His_6-Taf14-bound proteins were detected with antigen affinity-purified anti-Taf14 IgG (60). When His_6-Taf14 was omitted from the Far-Western blotting, the only signals observed were for purified Taf14 from the TFIID complex as well as trace amounts of Taf14 that co-purify with the yeast-generated MBP-Taf2. Upon overlay with His_6-Taf14, His_6-Taf14 bound to both Taf2 from TFIID and MBP-Taf2 but not MBP or other TFIID subunits. To extend these analyses to solution binding assays, increasing concentrations of MBP-Taf2 were mixed with either purified recombinant His_6-glutathione *S*-transferase (GST) or His_6-GST-Taf14 in the presence of BSA as a nonspecific competitor and subjected to GST pulldown. His_6-GST-Taf14 specifically bound MBP-Taf2 in a dose-dependent and saturable manner (Fig. 5*B*). Thus, we have shown through two independent methods that Taf2 and Taf14 specifically and directly interact *in vitro*.

The Taf2 C Terminus Is Necessary and Sufficient for Binding Taf14 in Vitro and in Vivo—Using the Far-Western blotting assay, we determined the domain of Taf2 where Taf2 and Taf14 directly interact (Fig. 6). To this end, purified MBP-Taf2 (*lane 1*), His_6-Taf2(1–407) (*lane 2*), His_6-Taf2(401–1007) (*lane 3*), His_6-Taf2(1001–1407) (*lane 4*), His_6-Taf2(1001–1207) (*lane 5*), and His_6-Taf2(1201–1407) (*lane 6*) were subjected to Far Western blotting as described above (Taf2-purified forms in Fig. 6*A*, *left*; constructs diagrammed in Fig. 6*B*). When His_6-Taf14 was omitted from the overlay, the only signal present was the co-purifying Taf14 in the MBP-Taf2 sample. Upon His_6-Taf14 overlay, His_6-Taf14 bound to MBP-Taf2 (*lane 1*), His_6-Taf2(1001–1407) (*lane 4*), and His_6-Taf2(1201–1407) (*lane 6*). These results suggest that the Taf14 binding domain resides in Taf2(1201–1407).

As described above, our systematic 100-aa *TAF2* truncation analysis showed that Taf2(1–1307) could complement a *taf2*-null strain and stably incorporate into the TFIID complex,

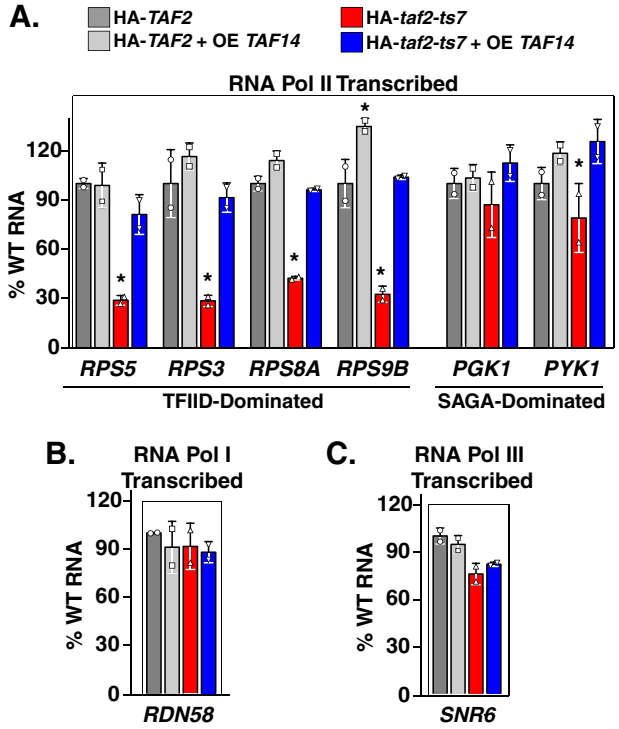

FIGURE 4. **Overexpression of *TAF14* suppresses the ribosomal protein gene transcription defect associated with *taf2-ts7*.** *A–C*, analysis of RNAs from cells shifted to the non-permissive temperature. Shuffled strains harboring HA_{x3}*NLS-TAF2* or HA_{x3}*NLS-taf2-ts7* with either an empty *HIS3*-marked overexpression (*OE*) plasmid or a *HIS3*-marked overexpression plasmid containing an N-terminally $FLAG_{x2}$NLS-tagged *TAF14* cDNA were grown at 25 °C to early to mid-log phase and then shifted to the non-permissive temperature (37 °C) for 2 h. RNAs were extracted and analyzed by qRT-PCR scoring for RNA Pol II- (*A*), RNA Pol I- (*B*), and RNA Pol III (*C*)-transcribed genes. Data were generated from two biological replicates. Each data point in the graph represents one biological replicate and is generated from the average of three technical replicates. Results were statistically analyzed using a two-way analysis of variance with Dunnett's multiple comparisons test (GraphPad Prism). Means ± S.D. (*error bars*) are depicted. *, $p < 0.05$. *Dark gray*, HA_{x3}*NLS-TAF2*; *light gray*, HA_{x3}*NLS-TAF2* + overexpressed *TAF14*; *red*, HA_{x3}*NLS-taf2-ts7*; *blue*, HA_{x3}*NLS-taf2-ts7* + overexpressed *TAF14*.

whereas Taf2(1–1207) could do neither (supplemental Table 1). Because these C-terminal amino acids contain the Taf14 binding domain, we hypothesized that a finer truncation analysis of the Taf2 C terminus may define the amino acids necessary for Taf14 binding *in vivo*. *TAF2* was subjected to 10-aa serial truncations of its C terminus. These variants were analyzed for their ability to complement a *taf2*-null strain, steady-state protein levels, and the ability to co-immunoprecipitate TFIID subunits (Fig. 6, *C* and *D*). We found that Taf2(1–1250) could not complement a *taf2*-null strain, had reduced steady-state protein levels compared with HA-Taf2, and could not co-immunoprecipitate TFIID subunits Taf4, Taf7, Taf8, Taf9, and Taf14. Smaller truncations (Taf2 aa 1–1260 to 1300) still maintained their ability to complement the *taf2*-null strain, displayed elevated steady-state protein levels compared with HA-Taf2, and could coimmunoprecipitate TFIID subunits Taf4, Taf7, Taf8, and Taf9. In regard to the Taf14 co-IP, Taf2(1–1280), Taf2(1–1290), and Taf2(1–1300) all maintained the ability to co-precipitate Taf14 at levels similar to WT. However, Taf2(1–1270) showed a mild reduction in the ability to co-precipitate Taf14, and Taf2(1–1260) (hereafter referred to as Taf2-ΔC) completely lost the ability to co-immunoprecipitate Taf14. Based on these data, we conclude that Taf2(1261–1407) is necessary for Taf2-Taf14 interaction *in vivo*.

Purified MBP-Taf2-ΔC was tested for its ability to directly interact with Taf14 *in vitro*. MBP-Taf2-ΔC was subjected to both Far Western blotting (Fig. 6*A*, *lane 7*) and GST pulldowns (Fig. 6*E*) as described above. MBP-Taf2-ΔC displayed no observable binding to His_6-Taf14 in the Far Western blot or His_6-GST-Taf14 in the GST pulldown. Thus, Taf2(1261–1407) is necessary for Taf14 binding *in vitro*.

To assess whether the Taf2 C terminus is sufficient for binding to Taf14 *in vivo*, untagged Taf2, HA-Taf2, HA-Taf2-ΔC, and HA-Taf2 C-terminal fragments (aa 1261–1407, 1271–1407, 1281–1407, 1291–1407, and 1301–1407) were subjected to α-HA co-IP as described above (Fig. 6*F*). As expected, HA-Taf2 could co-immunoprecipitate Taf7, Taf8, and Taf14, whereas HA-Taf2-ΔC could co-immunoprecipitate Taf7 and Taf8 but could not co-immunoprecipitate Taf14. Surprisingly, all of the Taf2 C-terminal fragments displayed the ability to co-immunoprecipitate Taf14. Despite Taf2(1261–1407) being necessary for binding to Taf14 *in vivo*, aa 1261–1407 and smaller C-terminal fragments are sufficient for binding to Taf14 *in vivo*. Considering that TFIID contains multiple copies of Taf14 per TFIID molecule (8), these data allowed us to hypothesize that the Taf2 C terminus contains multiple Taf14 binding domains that are independently capable of promoting Taf14-TFIID association.

Defining the Minimal Taf2 Interaction Domain in Taf14—In parallel to our analyses to map the Taf14 interaction domain in Taf2, Taf14 was also subjected to systematic truncation mutagenesis to identify the Taf14 domain operative in suppressing the *taf2-ts7* Ts phenotype. Previous Taf14 studies have shown that the N terminus contains the YEATS domain, whereas the Taf14 C terminus can both complement the growth deficiencies associated with a *taf14*-null strain and associate with transcription-related complexes such as TFIID and TFIIF *in vivo* (76). In addition, C-terminally tagged Taf14 variants display defects in growth, likely because the tag negatively impacts the ability of Taf14 to interact with transcription-related complexes (59).

In strains harboring *taf2-ts7*, Taf14 full length (aa 1–244), the Taf14 N terminus (aa 1–123), and the Taf14 C terminus (aa 124–244) were overexpressed to determine whether these fragments could suppress the Ts phenotype (Fig. 7*A*). All variants were expressed with a two-copy FLAG tag with an SV40 nuclear localization sequence ($FLAG_{x2}$NLS) N-terminal tag. Although Taf14(1–244) displayed the most robust suppression of the *taf2-ts7* Ts phenotype, Taf14(124–244) also suppressed the *taf2-ts7* Ts phenotype. The N-terminal YEATS domain-containing fragment (aa 1–123) could not suppress the *taf2-ts7* Ts phenotype. We further dissected the Taf14 C terminus in this overexpression suppression assay by performing systematic N- and C-terminal truncations of Taf14(124–244) (Fig. 7*A* and data not shown). These analyses identified that the domain minimally required for suppression of the *taf2-ts7* Ts phenotype lies within Taf14(164–244).

Again, the simplest model for the ability of the Taf14 C terminus to suppress the *taf2-ts7* Ts phenotype is that the C ter-

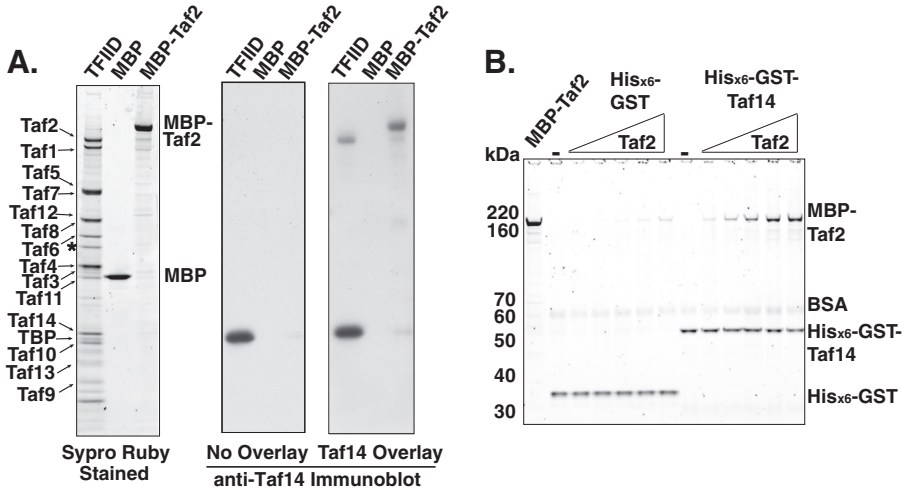

FIGURE 5. **Taf2 and Taf14 directly interact *in vitro*.** *A*, far-Western blotting. Approximately 500 ng of Taf1-TAP-purified TFIID, 200 ng of recombinant MBP, and 200 ng of recombinant MBP-Taf2 were separated via SDS-PAGE in triplicate. One gel was stained with SYPRO Ruby gel stain, whereas the other two were analyzed by anti-Taf14 blotting with and without 7 nM overlay of purified recombinant His_6-Taf14. A representative image is presented from more than three technical replicates. *B*, GST pulldowns. Either 4 pmol of purified recombinant His_6-GST or 2 pmol of His_6-GST-Taf14 were mixed with 0.1 mg/ml BSA and either no MBP-Taf2 or between 2 and 32 pmol of MBP-Taf2. His_6-GST- or His_6-GST-Taf14-bound proteins were pulled down with glutathione-agarose, washed with binding buffer, analyzed via SDS-PAGE, and stained with SYPRO Ruby gel stain. One picomole of purified MBP-Taf2 (*lane 1*) was loaded to demonstrate purity of input material. One technical replicate was performed.

minus of Taf14 directly interacts with Taf2. To test this hypothesis, purified recombinant His_6-GST, His_6-GST-Taf14(1–244), His_6-GST-Taf14(1–123), and His_6-GST-Taf14(124–244) were mixed with purified Taf2 and, in the presence of BSA, subjected to GST pulldown as described above (Fig. 7*B*). His_6-GST-Taf14(1–244) and His_6-GST-Taf14(124–244) were able to pull down purified Taf2 in a dose-dependent manner, whereas His_6-GST and His_6-GST-Taf14(1–123) did not pull down any detectable Taf2. These data confirm that the Taf14 C terminus, the domain required for suppression of the *taf2-ts7* Ts phenotype, is necessary and sufficient for direct interaction with Taf2 *in vitro*.

To identify point mutants that disrupt the *TAF2-TAF14* genetic interaction, we performed three-Ala scanning mutagenesis with 1-aa overlap of Taf14(164–244). These variants were overexpressed in the context of full-length Taf14 to determine whether they could suppress the *taf2-ts7* Ts growth phenotype. Of the 39 Ala variants generated, we identified 11 that displayed defects in the ability to suppress the *taf2-ts7*-associated Ts phenotype at 37 °C. The results of the suppression analyses for these 11 *taf14-ala* variants are summarized in Fig. 7*C*. A particularly sensitive hot spot was identified between Taf14 aa 218 and 230 where every mutant variant (m5–m10) displayed a defect in *taf2-ts7* Ts growth suppression. These amino acids are likely critical for the function of the Taf14 C terminus.

Fine Mapping of the Taf2 C Terminus Reveals Two Taf14 Interaction Domains—A previous study reported that the Taf2 C terminus is insoluble when expressed in *Escherichia coli* (59). Our studies confirm this observation. *E. coli* expressed Taf2(1301–1407)-His_6 is largely insoluble and refractory to native purification with Ni^{2+}-NTA-agarose (Fig. 8*C*, *lane 1*). We have previously shown that co-expression of insoluble Tafs with their cognate binding partner results in solubilization (47). Therefore, we hypothesized that co-expression of the Taf2 C terminus with either full-length Taf14 or Taf14(164–244) would result in solubilization of the Taf2 C-terminal fragment. To this end, we co-expressed Taf2(1301–1407)-His_6 with either Taf14(1–244) or Taf14(164–244) and subjected these complexes to Ni^{2+}-NTA-agarose purification. Using this strategy, we could generate soluble Taf2-Taf14 complexes in milligram quantities/liter of *E. coli* culture (Fig. 8, *A* and *B*, respectively). We also attempted to co-express full-length Taf2 with Taf14(164–244) in *E. coli*, but these attempts were unsuccessful (data not shown).

We then used this co-purification assay to fine-map the Taf14 binding domain within Taf2(1301–1407). N- and C-terminal truncations of Taf2(1301–1407)-His_6 were co-expressed with Taf14(164–244) in *E. coli* and subjected to Ni^{2+}-NTA-agarose purification (Fig. 8*C*; diagrammed in Fig. 8*D*). These analyses revealed that Taf2(1381–1407) were sufficient for Taf14 co-purification, whereas Taf2(1362–1407) were necessary for Taf14 co-purification. Henceforth, we will refer to Taf2(1363–1407) as Domain 1. Surprisingly, Domain 1 not only binds to Taf14 but also contributes to the insolubility of the Taf2(1301–1407) fragment because fragments deleted for Domain 1 can be purified from *E. coli* without co-purifying Taf14.

To assess the relevance of Taf2 Domain 1 to binding to Taf14 *in vivo*, we performed α-HA co-IPs with a series of Taf2 C-terminal deletion variants as described above (Fig. 8*E*). Considering that Taf2-ΔC (aa 1–1260) fails to interact with Taf14 *in vivo* and *in vitro* and that the Taf2(1301–1362)-His_6 fragment fails to co-purify Taf14, we reasoned that a second Taf14 binding domain likely resides within Taf2(1261–1300) (hereafter Domain 2). Deletion of either Domain 1 (Δ1) or Domain 2 (Δ2) had no impact on the ability of Taf2 to co-precipitate TFIID subunits Taf7, Taf8, and Taf14. However, a Taf2 double deletion variant (Δ1+Δ2) could co-precipitate Taf7 and Taf8 but failed to co-precipitate Taf14. Furthermore, successively smaller deletion within Domain 2 (Δ1261–1291, Δ1261–1281, and Δ1261–1271), when combined with Δ1, displayed strong

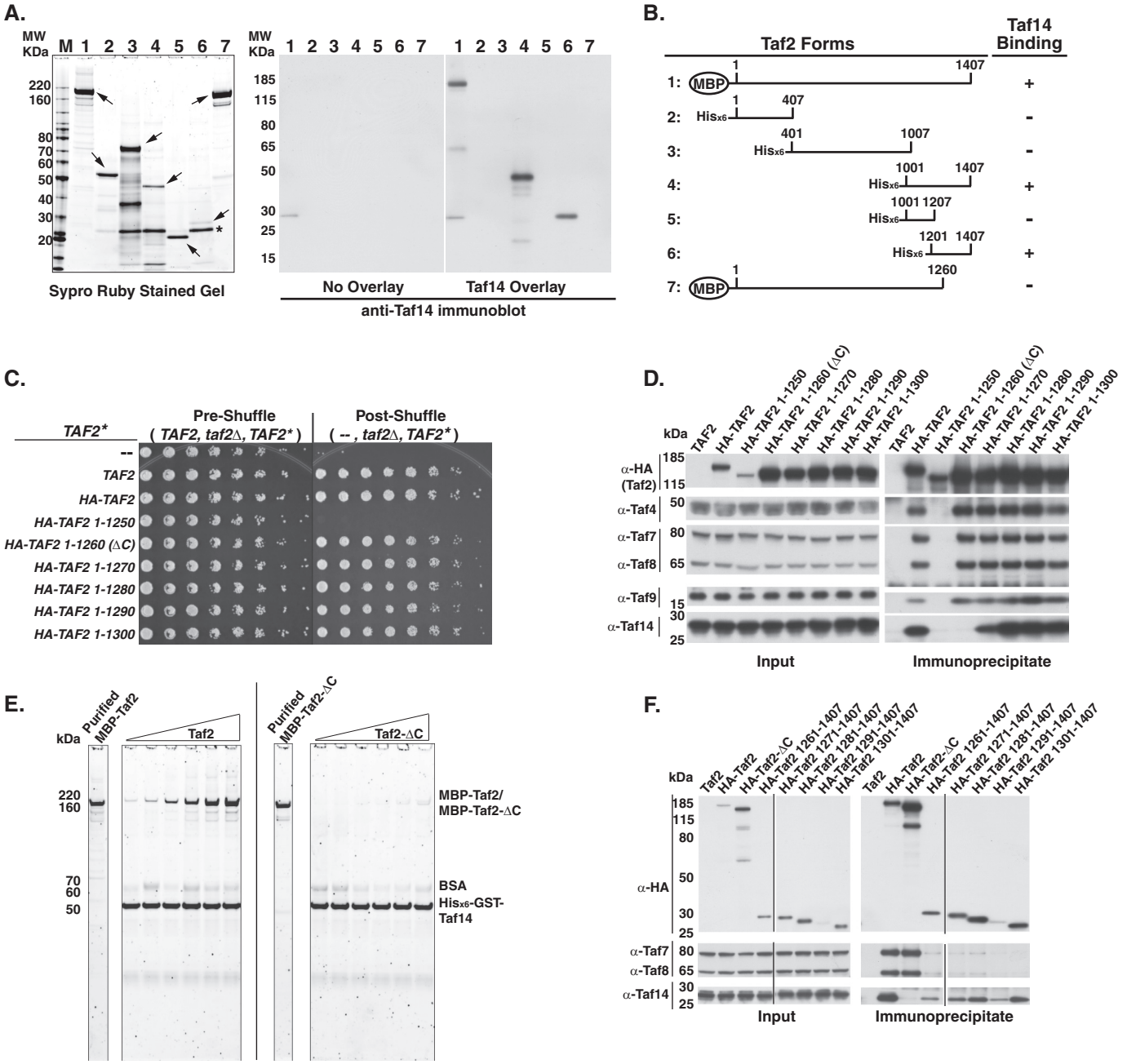

FIGURE 6. **The Taf2 C terminus is necessary and sufficient for binding to Taf14 *in vitro* and *in vivo*.** *A*, far Western blotting. Purified Taf2 forms were analyzed in triplicate as in Fig. 5 with one replicate analyzed by SYPRO Ruby gel staining (shown in *A*, *left*), whereas the other two were analyzed by anti-Taf14 far-Western blotting with and without His_6-Taf14 overlay (shown in *A*, *right*). Two technical replicates were performed. * indicates common *E. coli* protein contaminant. *B*, schematic of Taf2 forms used in *A*; *numbers* refer to the proteins loaded in *A*, *lanes 1–7*. *C* and *D*, plasmid shuffle complementation and Taf2-TFIID co-IP. Taf2 C-terminal truncation variants (*TAF2**: no ORF (−), *TAF2* full length aa 1–1407, HA_{x3}*NLS-TAF2* full length, and successive HA_{x3}*NLS-TAF2* truncation variants ranging from aa 1–1251 to aa 1–1300) were analyzed for their ability to complement a *taf2*-null strain via plasmid shuffle (*D*) and to co-immunoprecipitate TFIID subunits as described in Fig. 2. Additional anti-Taf IgGs were used in these analyses (α-Taf4 and α-Taf9). *E*, GST pulldowns. Similar to Fig. 5*B* except 5 pmol of His_6-GST-Taf14 were incubated with 0.1 mg/ml BSA and between 1 and 32 pmol of MBP-Taf2 or MBP-Taf2-ΔC. Two independent binding assays were performed, once with 2 pmol of His_6-GST-Taf14 and once with 5 pmol of His_6-GST-Taf14, both displaying high affinity saturable binding to MBP-Taf2 and a lack of specific binding to MBP-Taf2-ΔC. One picomole of purified MBP-Taf2 and 1 pmol of purified MBP-Taf2-ΔC were loaded to demonstrate purity of input material. *F*, Taf2-TFIID co-IP performed as described in Fig. 2. The *black line* depicts non-contiguous lanes from the same SDS-polyacrylamide gel and from the same film exposures. One technical replicate was performed. ΔC, Taf2(1–1260).

defects in the ability to co-precipitate Taf14. Taken together, these data are consistent with the Taf2 C terminus containing at least two distinct domains that can independently facilitate incorporation of Taf14 into the TFIID complex. Thus, to completely abrogate association of Taf14 with the TFIID complex, both of these domains must be disrupted.

The Taf14 Binding Domains in Taf2 Are Necessary for TAF14 Overexpression Suppression of the taf2-ts7 Growth Defect—Our overarching hypothesis has been that *TAF14* overexpression suppression of the *taf2-ts7* Ts phenotype occurs via a Taf2-Taf14 direct interaction. By extension, if Taf2 and Taf14 could no longer physically interact, then *TAF14* overexpres-

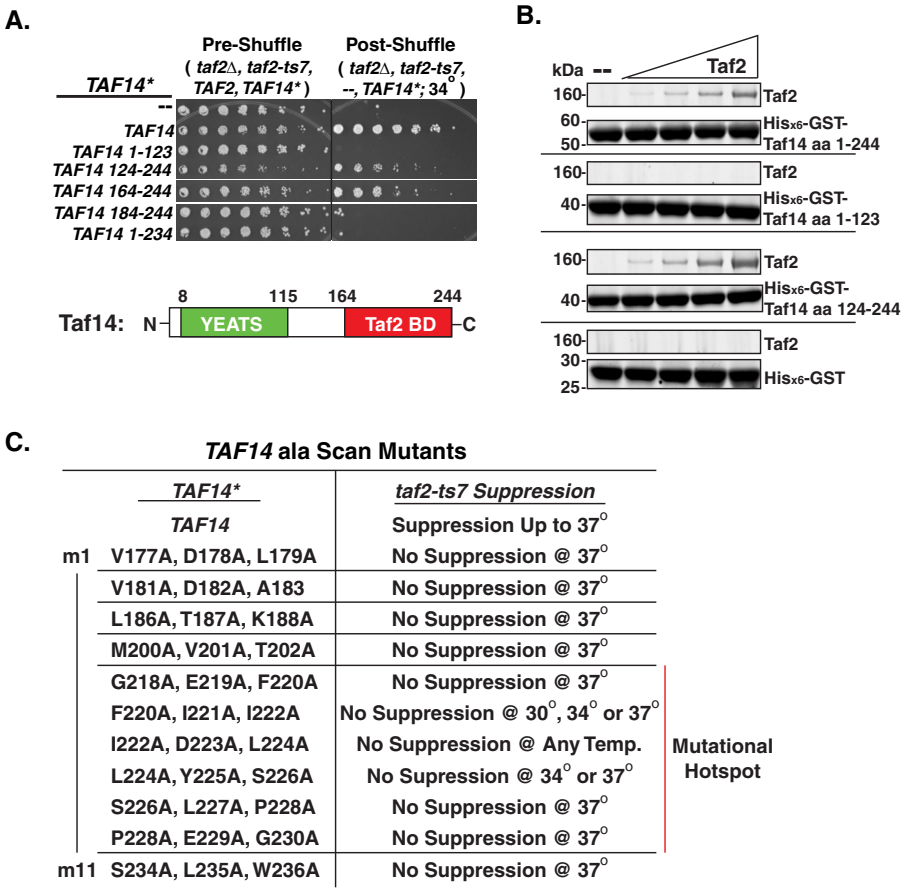

C.

***TAF14* ala Scan Mutants**

	*TAF14** *TAF14*	*taf2-ts7 Suppression*
		Suppression Up to 37°
m1	V177A, D178A, L179A	No Suppression @ 37°
	V181A, D182A, A183	No Suppression @ 37°
	L186A, T187A, K188A	No Suppression @ 37°
	M200A, V201A, T202A	No Suppression @ 37°
	G218A, E219A, F220A	No Suppression @ 37°
	F220A, I221A, I222A	No Suppression @ 30°, 34° or 37°
	I222A, D223A, L224A	No Suppression @ Any Temp.
	L224A, Y225A, S226A	No Supression @ 34° or 37°
	S226A, L227A, P228A	No Suppression @ 37°
	P228A, E229A, G230A	No Suppression @ 37°
m11	S234A, L235A, W236A	No Suppression @ 37°

Mutational Hotspot

FIGURE 7. **The Taf14 C terminus physically and functionally interacts with Taf2.** *A*, *TAF14* overexpression suppression of *taf2-ts7*. *Top*, plasmid shuffle performed as in Fig. 3*C*. *taf2*-null cells harboring a *URA3*-marked *TAF2* plasmid, a *LEU2*-marked HA_{x3}*NLS-taf2-ts7* plasmid, and a *HIS3*-marked *TAF14** overexpression plasmid (*TAF14* and *TAF14* N- and C-terminal truncation fragments; all *TAF14* forms contained an N-terminal $FLAG_{x2}$NLS tag) were spotted on SC −Leu,−His medium (*Pre-Shuffle*) or SC − Leu,−His + 5-FOA medium (*Post-Shuffle*) and grown for 72 h at 34 °C. A representative image of two biological replicates is presented. *Bottom*, schematic representing the domain structure of Taf14. Coordinates for YEATS domain were derived from Ref. 23. Coordinates for Taf2 binding domain (*BD*) were defined in this study. *B*, GST pulldowns. 16 pmol of purified recombinant His_6-GST, 8 pmol of His_6-GST-Taf14, 12 pmol of His_6-GST-Taf14(1–123), or 12 pmol of His_6-GST-Taf14(124–244) were mixed with 0.1 mg/ml BSA and either no Taf2 or 0.78, 1.56, 3.125, and 6.25 pmol of Taf2. His_6-GST- or His_6-GST-Taf14 variant-bound proteins were pulled down with glutathione-agarose, washed with binding buffer, analyzed via SDS-PAGE, and stained with SYPRO Ruby gel stain. One technical replicate was performed. *C*, summary of overexpression suppression of *taf2-ts7* with $FLAG_{x2}$*NLS-TAF14* Ala scan variants. *Horizontal lines* separate non-contiguous mutant variants. Results were derived from serial dilution spot assays as described in *A* (not shown). Two biological replicates were performed.

sion would no longer be able to suppress the *taf2-ts7* Ts phenotype.

To test this hypothesis, we performed genetic complementation assays with *TAF2*, *taf2*-Δ*C*, *taf2-ts7*, and *taf2-ts7*-Δ*C* with or without *TAF14* overexpression (Fig. 9*A*). As shown before, overexpression of *TAF14* did not have a strong impact on growth of strains harboring *TAF2*. However, overexpression of *TAF14* in strains harboring *taf2*-Δ*C* resulted in a synthetic slow growth phenotype. Similarly, although *TAF14* overexpression suppressed the *taf2-ts7* Ts phenotype, it did not suppress the *taf2-ts7*-Δ*C* phenotype but instead caused synthetic lethality. Consistent with our hypothesis, the Taf14 binding domains in the Taf2 C terminus are required for suppression of the *taf2-ts7* Ts phenotype.

Furthermore, our hypothesis also predicts that *TAF14* overexpression drives Taf2-Taf14 complex formation, resulting in stable incorporation into the TFIID complex. To test this hypothesis, we performed α-HA co-IP analysis as described above to determine the impact of *TAF14* overexpression on the ability of Taf2, Taf2-ΔC, Taf2-ts7, and Taf2-ts7-ΔC to co-precipitate TFIID subunits (Fig. 9*B*). The strains used for these analyses were pseudodiploid for both *TAF2*, containing WT and a test *TAF2* allele (*TAF2**), and *TAF14*, containing genomically encoded WT *TAF14* and either an empty overexpression plasmid or an expression plasmid containing $FLAG_{x2}$NLS-tagged *TAF14*. *TAF14* overexpression had no impact on the ability of Taf2 to co-immunoprecipitate Taf7 and Taf8; however, Taf2 co-precipitated elevated levels of Taf14 compared with the no-*TAF14* overexpression strain. Consistent with the synthetic sick growth phenotype, Taf2-ΔC reproducibly displayed a modest reduction in the ability to co-immunoprecipitate Taf7 and Taf8 in strains that overexpressed *TAF14*. Validating our hypothesis, *TAF14* overexpression rescued the ability of Taf2-ts7 to co-immunoprecipitate TFIID subunits Taf7, Taf8, and Taf14. However, Taf2-ts7-ΔC was not responsive to *TAF14* overexpression and still failed to efficiently co-immunoprecipitate TFIID subunits Taf7, Taf8, and Taf14.

Replacing the Taf14 Binding Domain in Taf2 with Taf14 via Gene Fusion Partially Suppresses the taf2-ts7-associated Growth Defects—Our data suggest that the domain necessary for Taf2-Taf14 interaction resides within Taf2(1261–1407),

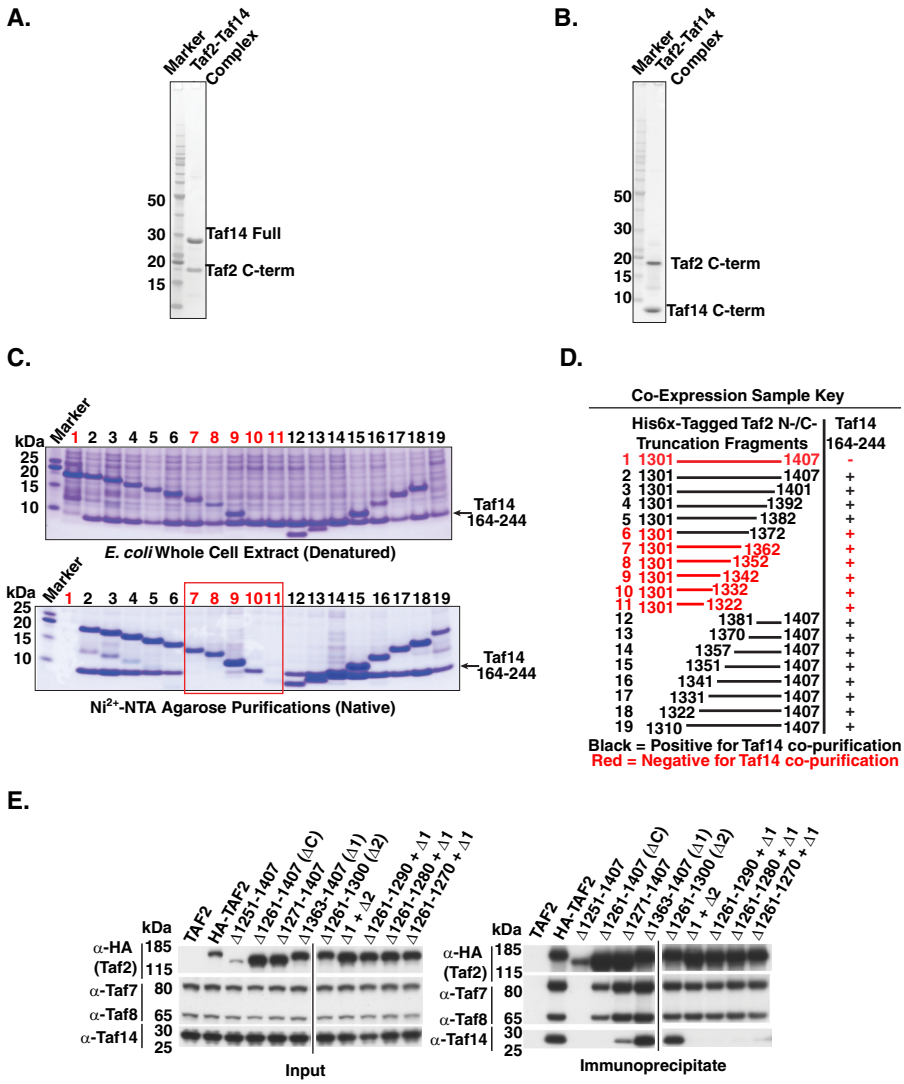

FIGURE 8. **Taf2 amino acids 1261–1407 contain two domains that contribute to Taf14 binding.** *A* and *B*, co-purification of Taf2 and Taf14. Taf2(1301–1407)-His_6 was co-expressed in *E. coli* with either Taf14(1–244) or Taf14(164–244) and purified using Ni^{2+}-NTA-agarose. Purified Taf2(1301–1407)/Taf14(1–244) (shown in *A*) and Taf2(1301–1407)/Taf14(164–244) (shown in *B*) were separated via SDS-PAGE and stained with Coomassie Blue. *C* and *D*, fine mapping of the Taf14 interaction domain in Taf2(1301–1407). C-terminally hexahistidine-tagged Taf2(1301–1407) and N- and C-terminal truncation variants of Taf2(1301–1407) (diagrammed in *D*) were co-expressed with Taf14(164–244) in *E. coli*. As a negative control, C-terminally hexahistidine-tagged Taf2(1301–1407) was expressed alone. Denatured whole cell extracts or Ni^{2+}-NTA-agarose-purified complexes were separated on SDS-PAGE and stained with Coomassie Blue (*C*). Samples that co-purify Taf14(164–244) are shown in *black*, whereas samples that fail to co-purify Taf14(164–244) are shown in *red*. A representative image of two technical replicates is shown. *E*, Taf2-TFIID co-IP performed as described in Fig. 2. All deletion variants contain an HA_{x3}NLS tag. *Black lines* separate non-contiguous lanes from the same SDS-polyacrylamide gel and from the same film exposures. One technical replicate was performed. ΔC, deletion of Taf2(1261–1407); Δ1, deletion of Taf2(1363–1407); Δ2, deletion of Taf2(1261–1300).

whereas the location of the mutations in *taf2-ts7* and *-ts8* reside between Taf2 aa 1100 and 1150. Based on this discrepancy, we conceived of two possible mechanisms through which *TAF14* overexpression can suppress the growth phenotypes associated with these Ts mutants. First, saturating the C terminus of Taf2-ts7 and -ts8 with Taf14 induces a conformational change that allows these variants to more stably associate with the TFIID complex. Second, when at saturating levels, Taf14 can tether Taf2-ts7 and -ts8 to the TFIID complex, likely through direct interaction between Taf14 and another TFIID subunit(s). The first model inherently requires a binding event where Taf14 binding to Taf2-ts7 or -ts8 induces a conformational change. The second model involves Taf14 playing a role outside of simply Taf2 binding.

To distinguish between these two models, we constructed Taf2-Taf14 chimeras where *taf2-ΔC* and *taf2-ts7-ΔC* were fused to the *TAF14* ORF. Ideally, these chimeric fusions would bypass the need for *TAF14* overexpression to achieve saturable binding to the Taf2 C terminus because these chimeras contain covalently attached Taf14. These chimeras were tested to see whether they could complement a *taf2*-null strain (Fig. 10*A*). A "WT" chimera (*taf2-ΔC-Taf14*) supported growth at a level similar to *TAF2*, suggesting the chimera does not negatively impact Taf2 function. This *taf2-ts7-ΔC-TAF14* chimera suppressed the slow growth phenotype at 30 °C associated with *taf2-ts7* and *taf2-ts7-ΔC*.

We then sought to determine whether this suppression was Taf14-dependent and, if so, which domain(s) was involved. To

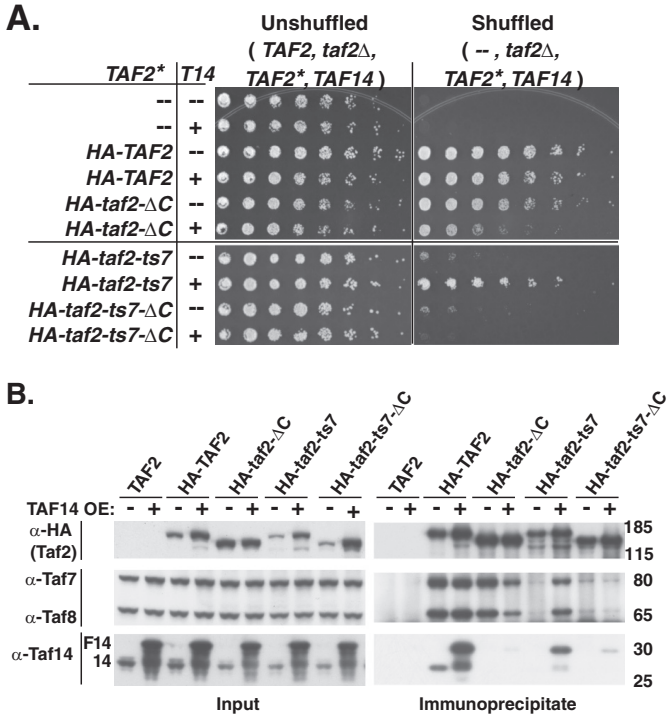

FIGURE 9. **The Taf14 binding domain in Taf2 is necessary for *TAF14* overexpression-mediated suppression of *taf2-ts7*.** *A*, intragenic *TAF2* synthetic genetics. Plasmid shuffle complementation assays were performed as described in Fig. 3*C*. Cells were grown for 72 h at 25 °C prior to imaging. Representative images from at least two biological replicates are presented (*TAF2**: no ORF (−), *TAF2*, HA_{x3}*NLS-TAF2*, HA_{x3}*NLS-TAF2-ΔC*, HA_{x3}*NLS-taf2-ts7*, and HA_{x3}*NLS-taf2-ts7-ΔC*). *B*, Taf2-TFIID co-immunoprecipitation performed as described in Fig. 2 except that strains also contained either an empty *HIS3*-marked overexpression (*OE*) plasmid or a $FLAG_{x2}$*NLS-TAF14* cDNA containing *HIS3*-marked overexpression plasmid. A representative image of at least two biological replicates is shown (*TAF2**: no ORF (−), *TAF2*, HA_{x3}*NLS-TAF2*, HA_{x3}*NLS-TAF2-ΔC*, HA_{x3}*NLS-taf2-ts7*, and HA_{x3}*NLS-taf2-ts7-ΔC*). Taf14 WT is labeled *14*; $FLAG_{x2}$NLS-Taf14 is labeled *F14*.

this end, we made *taf2-ts7-ΔC-taf14* chimeras with mutations either in the Taf2 binding domain of Taf14 (*taf14-m3*; L186A,T187A,K188A) or in the Taf14 YEATS domain that disrupt its ability to bind to acetylated or crotonylated H3K9 (*taf14-W81A* and *taf14-G80K*) (23, 24). Mutations in the Taf14 C terminus completely abrogated the ability of the chimera to suppress the growth defect associated with *taf2-ts7-ΔC*. In addition, whereas both YEATS domain mutant fusions displayed some reduction in the ability to suppress the growth defects associated with *taf2-ts7-ΔC*, the G80K mutation displayed a significant loss in the ability to suppress. The loss of suppression cannot be attributed to a reduction in steady-state protein levels because all constructs were expressed at least as well as WT Taf2 (Fig. 10*B*).

TAF14-less TFIID Mutant Cells Display a Slow Growth Phenotype and Defects in RPG Transcript Abundance—Our results suggest that the Taf2 C terminus is not only required for Taf2-Taf14 interaction but is also required for association of Taf14 with the TFIID complex. To test this hypothesis, we engineered two strains: one that genomically encodes an HA_{x1} tag at the N terminus of Taf1 for anti-HA immunopurification and one that encodes both an HA_{x1}-Taf1 and genomic deletion of Taf2(1261–1407). TFIID was purified from these two strains as described previously (8) and then subjected to SDS-PAGE and gel staining to score TFIID subunit composition and stoichiometry (Fig. 11*A*). When comparing the TFIID variants, two differences were apparent. First, in the Taf2-ΔC TFIID, the size of Taf2 was reduced, reflecting the genomic Taf2 C-terminal deletion. However, Taf2-ΔC is maintained at an apparent 1:1 Taf2-TFIID stoichiometric ratio relative to Taf1, similar to HA_{x1}-Taf1 TFIID, indicating that the deletion does not negatively impact the stability of Taf2 in the TFIID complex. Second, in the Taf2-ΔC TFIID, Taf14 is completely absent, consistent with our Taf2 C terminus truncation analyses. Quantitation of these TFIID preparations demonstrates that the stoichiometry for the rest of the TFIID subunits is similar between the two TFIID forms. Based on these data, we can conclude that Taf2(1261–1407) is necessary for Taf14 stable incorporation into the TFIID complex and that strains lacking Taf2(1261–1407) have TFIID devoid of Taf14 (Taf14-less TFIID).

When we streaked these TFIID purification strains onto rich medium to isolate single colonies, we found that the Taf14-less TFIID strain displayed a reduced growth rate as measured by colony size (data not shown). To determine whether this phenotype was directly attributable to the Taf2-ΔC variant, growth curves were performed in yeast strains that contain only *HA-TAF2* or *HA-taf2-ΔC*. These growth curves revealed that strains harboring *HA-TAF2-ΔC* displayed a 14.5-min (15.6%) slower growth rate during log phase at 30 °C (Fig. 11*B*).

We then assessed steady-state transcript abundance for these two strains. RNA was extracted from mid-log phase cells growing at 25 °C and analyzed using qRT-PCR. Despite no reduction in transcript abundance for RNA polymerase I-transcribed *RDN58* (Fig. 11*D*) and RNA polymerase III-transcribed *SNR6* (Fig. 11*E*), we reproducibly observed a statistically significant ~2-fold reduction in RPG transcript abundance (*RPS5*, *RPS9B*, *RPS8A*, and *RPS3*) (Fig. 11*C*). In addition, we observed a moderate (~25%), although not statistically significant for both genes, reduction in steady-state transcript abundance for the SAGA-dominated glycolytic *PGK1* and *PYK1* genes. Although the glycolytic genes are not considered TFIID-dependent, our data are consistent with previously observed modest reductions in *PGK1* steady-state transcripts in $taf4^{ts}$ variants (32).

Discussion

Multiple structural and biochemical studies have attributed specific Tafs with promoter-DNA or modified chromatin binding capabilities (10–12, 15, 16, 18, 19, 21, 23, 24, 37, 56). These activities provide convenient mechanisms through which TFIID can engage with genes to facilitate PIC formation. Indeed, an activator-TFIID-TFIIA promoter-DNA quaternary complex with distinct TFIID-DNA interactions displays a locked DNA conformational state that likely serves as a platform for general transcription factor and Pol II binding (57). However, these many biochemical activities have rarely been interrogated genetically to establish their importance *in vivo* (37). This lack of knowledge was the impetus for the work reported here.

Specifically, the functional role of Taf2 *in vivo* was largely unknown despite longstanding evidence for its *in vitro* INR binding activity (12, 18, 19). A lack of Taf2 molecular genetic

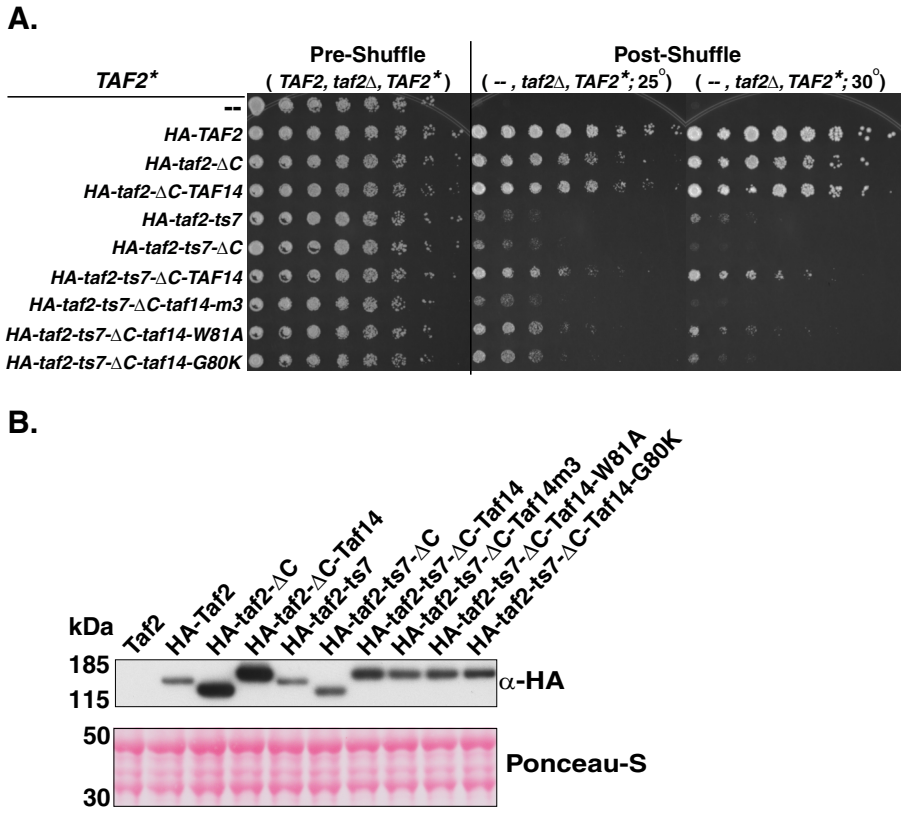

FIGURE 10. **Replacing the Taf14 binding domain in Taf2 with Taf14 partially suppresses the *taf2-ts7* growth defect.** *A*, plasmid shuffle genetic complementation performed as described in Fig. 2. Cells were grown for 60 h at 25 and 30 °C prior to imaging. Plate images are representative of at least two biological replicates (TAF2*: no ORF (−), *TAF2*, HA_{x3}*NLS-TAF2*, HA_{x3}*NLS-TAF2-ΔC*, HA_{x3}*NLS-TAF2-ΔC-TAF14* chimeric fusion, HA_{x3}*NLS-taf2-ts7*, HA_{x3}*NLS-taf2-ts7-ΔC*, HA_{x3}*NLS-taf2-ts7-ΔC-TAF14* chimeric fusion, HA_{x3}*NLS-taf2-ts7-ΔC-taf14 m3* chimeric fusion, HA_{x3}*NLS-taf2-ts7-ΔC-taf14-W81A* chimeric fusion, and HA_{x3}*NLS-taf2-ts7-ΔC-taf14-G80K* chimeric fusion). *B*, steady-state protein immunoblot. Total cell protein was fractionated via SDS-PAGE and transferred to PVDF membrane. The high molecular weight part of the membrane was probed with anti-HA antibody, and total protein on the lower molecular weight part of the membrane was visualized with Ponceau S as a loading control.

studies is likely a result of technical challenges. In addition to being essential for life, Taf2 is a large protein and particularly labile in ScTFIID purifications (41, 61). As our study demonstrates, systematic deletion analyses largely disrupt Taf2 protein stability and the ability of Taf2 to stably incorporate into the TFIID complex, precluding conventional methods of genetically interrogating large proteins (supplemental Table 1) (70, 71, 77). Our site-directed mutagenesis approach generated variants that displayed similar TFIID incorporation defects, limiting our ability to interpret their precise molecular functions (Fig. 2). Of note, while this manuscript was in preparation, specific amino acids were predicted to be important for the INR binding function of Taf2 (68). One of the site-directed mutants generated in this study, *taf2-m32*, targeted a subset of these residues but displayed only a mild slow growth phenotype and was not further pursued (supplemental Table 2). Genetic interrogation of this putative INR binding domain will likely shed insights into the role of INR binding in TFIID transcriptional activation.

Our key finding in this report is the discovery of a genetic interaction between *TAF2* and *TAF14*. Individual overexpression of each TFIID subunit identified *TAF14* overexpression as a mechanism to achieve suppression of select $taf2^{ts}$ alleles (*taf2-ts7* and *-ts8*). The location of the residues mutated in these Ts variants is suggestive of a functional domain. Furthermore, we demonstrate that Taf2 and Taf14 directly interact. Molecular genetic dissection of both Taf2 and Taf14 led to the identification of the domains responsible for physical and functional interaction *in vivo* and *in vitro*.

Our previous structural and biochemical characterization of the TFIID complex identified the stoichiometry and location of all of the TFIID subunits with the exception of Taf14 (8, 40–42). Purified TFIID displays a stoichiometry of at least two copies of Taf14 per TFIID molecule. In addition, Taf14 self-associates *in vivo*. However, gel staining of purified SWI/SNF and TFIIF show one copy per complex so this multicopy per complex phenotype is likely to be specific to TFIID (52, 58). Although deletion of the Taf2 C terminus completely disrupts association of Taf14 with the TFIID complex, fine mapping of the Taf2 C terminus identified two domains that can independently facilitate Taf14 incorporation into the TFIID complex. These data are consistent with a genome-wide two-hybrid screen, which identified part of the Taf2 C terminus as a Taf14-interacting protein (59). However, Taf2 variants that fail to stably incorporate into the TFIID complex as well as Taf2 C-terminal fragments display reductions in Taf14 co-precipitation relative to WT Taf2. This observation suggests that when Taf2 incorporates into the TFIID complex Taf14 binding is enhanced, potentially through a multivalent binding site between Taf2 and another TFIID subunit(s).

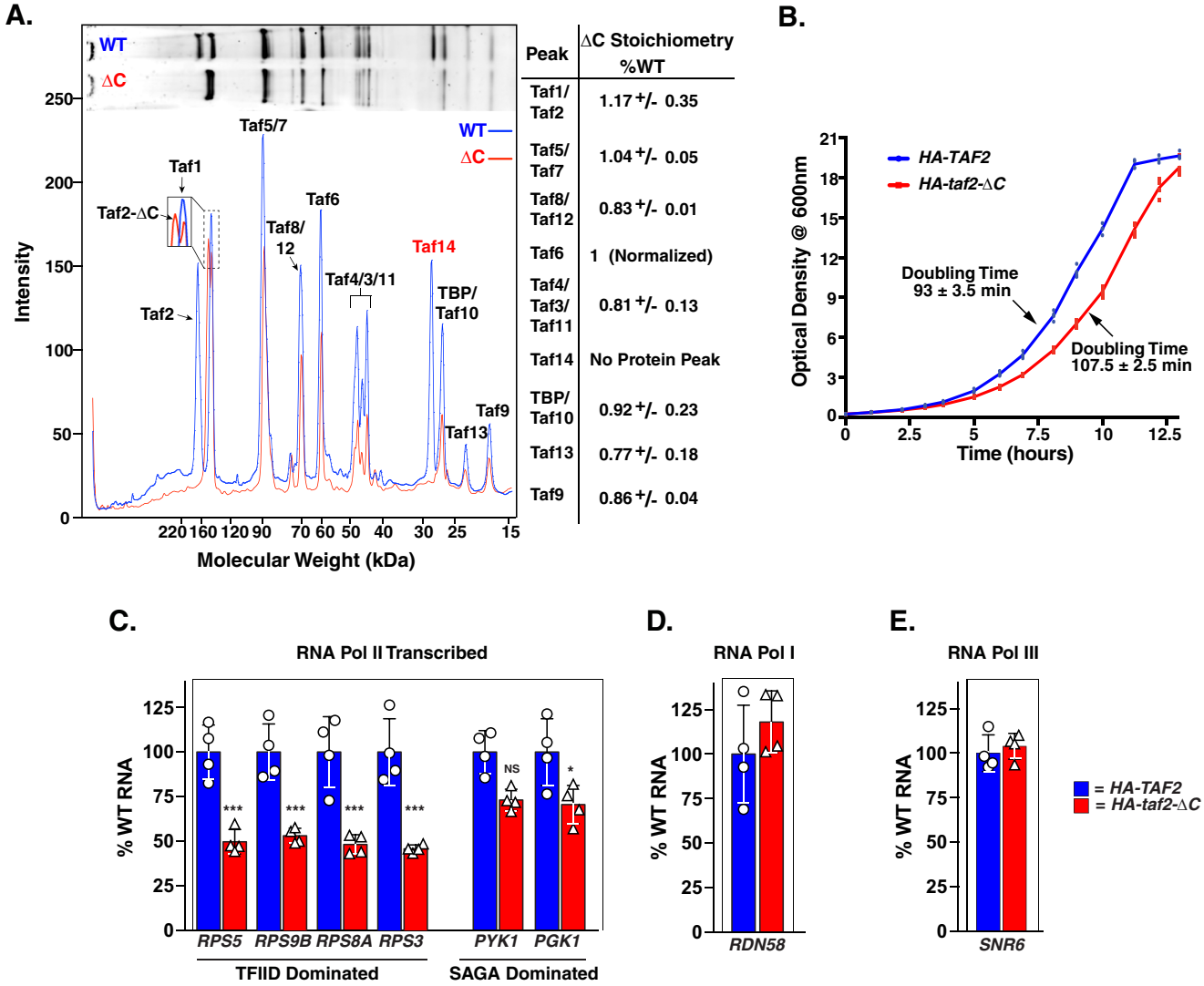

FIGURE 11. **Taf14-less TFIID mutant cells display a slow growth phenotype and defects in ribosomal protein gene transcription.** *A*, purified TFIID forms. Between 300 and 600 ng of HA_{x1}-Taf1-purified TFIID and HA_{x1}-Taf1 Taf2-ΔC-purified TFIID were separated via SDS-PAGE and stained with SYPRO Ruby gel stain. Peak traces were generated using Quantity One (Bio-Rad). TFIID subunit peaks were quantified in ImageJ by calculating the area under the curve. The signal intensity of Taf6 was used to normalize each TFIID preparation to determine relative subunit stoichiometry for each peak. Means ± S.D. are depicted. Quantitation was generated from two technical replicates. *B*, growth rate analysis. Log phase growing *taf2*-null cells shuffled to contain either plasmid-borne HA_{x3}*NLS-TAF2* or plasmid-borne HA_{x3}*NLS-TAF2*-Δ*C* were diluted to an OD_{600} of ~0.2 (HA_{x3}*NLS-TAF2*, average start OD_{600} of 0.229; HA_{x3}*NLS-TAF2*-Δ*C*, average start OD_{600} of 0.239) and grown at 30 °C, and OD_{600} was measured approximately every hour until the strains reached stationary phase growth. Doubling time was calculated using a non-linear exponential growth fit (GraphPad Prism) for the early phase of the growth curve (first seven time points). A growth curve was performed with four biological replicates. Experimental error in doubling time is derived from S.E. *C*, *D*, and *E*, qRT-PCR. Steady-state RNA was analyzed by qRT-PCR scoring for RNA Pol II- (*C*), RNA Pol I- (*D*), and RNA Pol III (*E*)-transcribed genes. Data were generated from four biological replicates. Each data point in the graph represents one biological replicate and is generated from the average of three technical replicates. Results were statistically analyzed using a two-way analysis of variance with Sidak's multiple comparison test (GraphPad Prism). Means ± S.D. (*error bars*) are depicted. *, $p < 0.05$; ***, $p \leq 0.0001$. *Blue*, shuffled strain harboring plasmid-borne HA_{x3}*NLS-TAF2*; *red*, shuffled strains harboring plasmid-borne HA_{x3}*NLS-TAF2*-Δ*C*.

Interestingly, the Taf2 domain identified to directly interact with Taf14 does not contain the amino acids mutated in *taf2-ts7* or *-ts8* despite this domain being required for *TAF14* overexpression suppression of these variants. To test the possibility of a multivalent Taf14 binding site between Taf2 and another TFIID subunit, we fused *TAF14* to a $taf2^{ts}$ variant deleted for the Taf14 binding domain. This chimeric fusion improved growth in a *TAF14*-dependent manner consistent with the existence of a multivalent binding site. The TFIID subunit responsible is likely to be Taf8. Human Taf2 directly interacts with Taf8 (44). Taf1-TAP purifications of TFIID result in substoichiometric levels of Taf2, Taf8, and Taf14 (41). Furthermore, specific deletions in Taf1 result in dissociation of Taf2, Taf8, and Taf14 from the TFIID complex, suggesting that these three subunits form a subcomplex (70). As with human TFIID, the association of Taf2 and Taf8, along with Taf14, with the TFIID core may stimulate a structural transition in the TFIID assembly pathway (43).

The function of Taf14 in transcription regulation has remained enigmatic. Functional interpretation of *TAF14* mutant variants is limited because of its presence in multiple transcription-related complex assemblies (52, 58–60). Specifically, molecular defects in *taf14*-null strains or strains harboring *taf14* mutant variants unable to bind modified H3K9 could

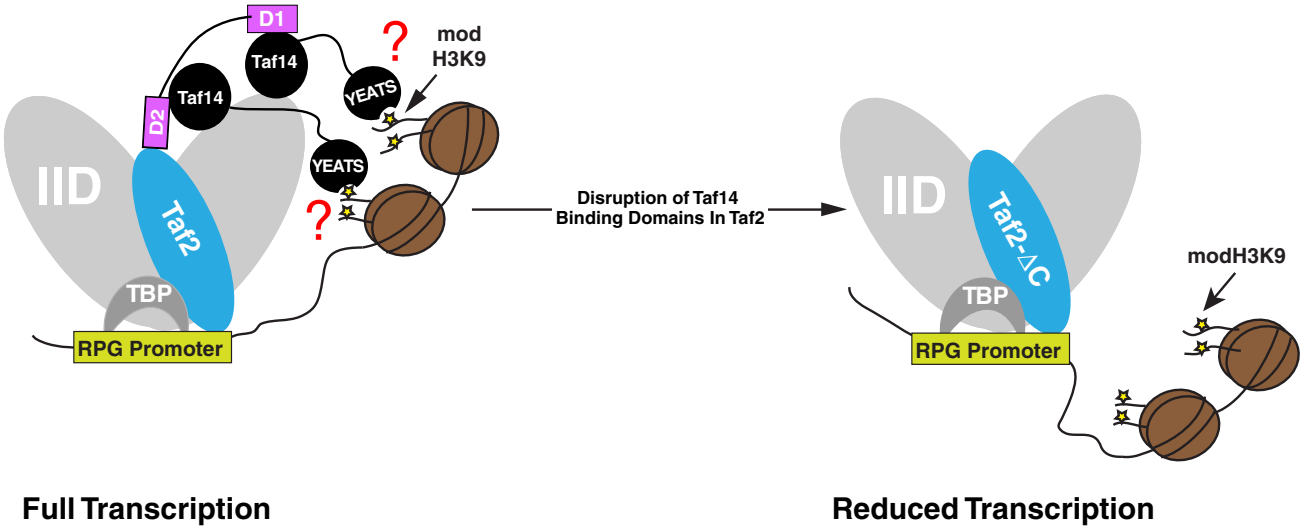

FIGURE 12. **Model of Taf2-Taf14 interaction in TFIID-dependent transcription.** *Left*, depicts role of Taf2 C terminus in facilitating incorporation of two Taf14 molecules per TFIID complex. Taf14 may then bind to active chromatin through its YEATS domain. *Brown circles*, histone octamer; *yellow stars*, modified (*mod*) H3K9; *D1*, Taf2 Taf14 binding Domain 1; *D2*, Taf2 Taf14 binding Domain 2. *Right*, Taf14 cannot incorporate into the TFIID complex, and as a result TFIID may lose the ability to communicate with active chromatin through the Taf14 YEATS domain.

be attributed to TFIID-promoter interactions, the role of TFIIF in PIC or elongation function, ATP-dependent chromatin remodeling, or the myriad transcription-related functions associated with Mediator. Our study begins to decipher the role of Taf14 in transcription regulation through the identification of *taf2-ΔC*, a separation-of-function Taf2 variant that can stably incorporate into the TFIID complex but precludes incorporation of Taf14. The existence of this variant is consistent with the model presented by Kabani *et al.* (59) that Taf14 has a particular entry point protein in each complex with which it is associated. Thus, it may be possible to generate genetic reagents that specifically dissociate Taf14 from the TFIIF, Ino80 (inositol-requiring complex), Swi/Snf, NuA3 (nucleosome acetyltransferase complex 3), Mediator, and RSC without perturbing complex integrity or the other functions of the complex. *taf2-ΔC* mutant cells display a modest slow growth phenotype as well as a reduction in transcript abundance for the TFIID-dominated RPGs. In addition, purification of TFIID from strains harboring *taf2-ΔC* yields a Taf14-less TFIID complex. Structural analyses of this complex in contrast with WT TFIID may yield important insights into the location of Taf14 in TFIID as well as the mechanism by which two copies of Taf14 can associate with a single TFIID molecule.

Our data suggest that *taf2-ΔC* is a true separation-of-function variant whose cellular and molecular phenotypes reflect the contribution of Taf14 to TFIID function (Fig. 12). However, the mechanism by which Taf14 contributes to TFIID transcription activation mechanism remains speculative. The Taf14 YEATS domain responsible for binding to modified chromatin (23, 24) may enhance TFIID occupancy of active genes by increasing the number of contact points between TFIID and gene promoters. In addition, our Taf2-Taf14 chimeric fusion analyses suggest that the YEATS domain does contribute to TFIID function, likely through its ability to interact with modified chromatin. This hypothesis is consistent with the observation that the Taf3 PHD finger H3K4me3 binding activity stimulates transcription, especially in the context of a mutant TATA box (37). Similar *in vitro* transcription experiments with chromatin templates need to be performed with WT and Taf14-less TFIID to assess the validity of this model for ScTFIID considering that the Taf3 PHD finger is not present in the yeast system.

In contrast, the Taf14 YEATS domain is non-essential and displays minimal growth defects when deleted, whereas deletion of the Taf14 C-terminal domain phenocopies the *taf14*-null strain (76). Considering the Taf14 C-terminal domain is responsible for the interaction with Taf14-associated complexes, this domain could mediate interactions among these complexes that have thus far not been explored. We do not know whether a single Taf14 molecule can bind to multiple transcription-related complexes at the same time or whether binding of Taf14 to TFIID or TFIIF, for example, is mutually exclusive. If these interactions are not mutually exclusive, Taf14 could serve as a bridge between the transcription machinery that could play a key role in the transcription process.

In summary, through systematic mutagenesis of the TFIID subunit Taf2, we have uncovered important physical and functional interactions between Taf2 and Taf14. These discoveries have shed light on the role Taf14 plays in TFIID function including a putative role in TFIID-chromatin interaction. We believe our study could provide a model for disambiguating the role Taf14 plays in gene regulatory mechanisms.

Materials and Methods

Bacterial Strains and Cloning—E. coli DH5α was used for all cloning and propagation of plasmids. Recombinant proteins were expressed in *E. coli* Rosetta2 (DE3) strains (Novagen). All cloning was performed using restriction enzyme-based methods. Appropriate restriction ends were added to all cloned sequences using PCR with either *Pyrococcus woesei* DNA polymerase as described (78) or Q5 DNA polymerase according to the manufacturer's instructions (New England Biolabs). Site-directed mutagenesis was performed using gene splicing

by overlap extension PCR (79). All constructs were sequence-verified.

Yeast Manipulations—Strains were grown in YPD (1% (w/v) yeast extract, 2% (w/v) peptone, 2% (w/v) dextrose) or synthetic complete medium (SC) (0.67% (w/v) yeast nitrogen base without amino acids, 2% (w/v) dextrose (or 1% (w/v) raffinose where indicated), 0.2% (w/v) amino acid dropout mixture) without (−) leucine (Leu), histidine (His), or uracil (Ura) or a combination of the three where appropriate as indicated. All transformations were performed using the lithium acetate/PEG/salmon sperm carrier DNA transformation protocol (80). For plasmid shuffle assays, cells were grown on SC −Leu, −His, or both including 0.1% 5-fluoroorotic acid (5-FOA) (81).

All strains generated in this study were derivatives of BY4741 (82). Yeast expression vectors were derivatives of shuttle vectors described by Mumberg *et al.* (83, 84) A *taf2*-null strain (JFTAF2del) was generated by co-transforming BY4741 with a p416ADH *TAF2* covering plasmid and a linearized *TAF2* deletion cassette. The *TAF2* deletion cassette replaced −233 to +4224 relative to the start codon of the *TAF2* ORF with the hygromycin B resistance cassette from pAG32 (85). Co-transformants were sequentially plated on SC −Ura followed by replica plating to YPD + 300 μg/ml hygromycin B. Hygromycin B^+ and Ura^+ clonal isolates were confirmed as *taf2*-null using plasmid shuffle genetic complementation. An HA_{x1}-TAF1 strain (JFHATAF1) was generated using ends-in integration of an *HA_{x1}-TAF1* N-terminal tagging cassette into the *TAF1* locus using a similar strategy described previously for Mot1 (86). The resulting strain harbors a $G418^R$ cassette and an N-terminal MYPYDVPDYAGVE tag (HA epitope underlined) at the *TAF1* chromosomal locus (additional details are available upon request). JFHAT1T2delC was generated by applying PCR-based homologous recombination methods to *TAF2*, deleting sequences coding for amino acids 1261–1407 at its chromosomal locus. The Taf2-ΔC deletion was confirmed by PCR and immunoblotting.

I-TASSER Structural Prediction and TAF2 Site-directed Mutagenesis—Primary amino acid sequences for *S. cerevisiae* (yeast) Taf2, *Drosophila melanogaster* (fly) Taf2, and *Homo sapiens* (human) Taf2 were submitted to the I-TASSER server for 3D structure prediction (72). Resulting 3D models of yeast, fly, and human were imported in PyMOL, displayed in cartoon format and colored based on secondary structure. The first of five models generated for yeast Taf2 was used to define predicted solvent-exposed residues.

To assess amino acid conservation, yeast, fly, and human Taf2 primary sequences were aligned in MacVector using ClustalW. Fifty-eight mutants were designed based on solvent accessibility and proximity to amino acids that are either similar or identical among yeast, fly, and human Taf2. Twenty-nine additional mutants were designed based on amino acids predicted to be solvent-inaccessible but highly conserved among yeast, fly, and human Taf2. All mutations were arbitrarily limited to a maximum of 8 contiguous amino acids. A list of the mutants is provided (supplemental Table 2).

Plasmid Shuffle and Overexpression Suppression—All *TAF2* site-directed mutants, deletion mutants, and *TAF2-TAF14* chimeras were expressed from p415ADH with an N-terminal HA_{x3}NLS (additional details are available upon request). For plasmid shuffle analyses, JFTAF2del was transformed with an empty p415ADH plasmid, a p415ADH-*TAF2* plasmid, a p415ADH-*HA_{x3}NLS-TAF2* plasmid, or a p415ADH-*HA_{x3}NLS-TAF2* mutant plasmid, and transformants were grown on SC −Leu plates. Leu^+ colonies were grown to saturation in SC −Leu at 30 °C, serially diluted 1:4 in sterile H_2O, spotted to SC −Leu or SC −Leu + 5-FOA 15-cm plates using a pinning tool, and grown at various temperatures (20, 25, 30, 34, and 37 °C) to assess temperature-sensitive growth. Duration of growth ranged from 48 to 96 h as indicated.

For overexpression suppression screening of all TFIID subunits, the ORFs of *TAF1–TAF14* and *SPT15* (TBP) were cloned into p413GPD using varied restriction ends (details are available upon request). Plasmid shuffle analyses were performed essentially as above with the following exception. JFTAF2del was co-transformed with *LEU2*-marked *TAF2* plasmids and an empty p413GPD or p413GPD containing the ORF for each of the TFIID subunits and grown on SC −His,−Leu plates. For each *LEU2*-marked *TAF2* and p413GPD TFIID subunit combination, two His^+Leu^+ colonies were spotted undiluted to SC −His,−Leu or SC −His,−Leu + 5-FOA. TFIID subunits that scored positive for overexpression suppression displayed uniformly improved growth for both colonies tested.

For directed overexpression suppression studies with *TAF14*, both WT and mutant *TAF14* variants were expressed with an N-terminal $FLAG_{x2}$NLS.

Immunoblotting and Co-immunoprecipitation—For steady-state protein immunoblotting, protein was extracted from approximately 1.2×10^7 cells of early to mid-log phase-grown culture using sodium hydroxide-based lysis (87). For co-immunoprecipitations, JFTAF2del strains were grown as pseudodiploids containing both a wild-type *URA3*-marked *TAF2* gene and a WT or mutant *LEU2*-marked *TAF2* gene. In these analyses, 50 ml of yeast cells were grown at 30 °C to early to mid-log phase (approximately $2.4–3.6 \times 10^7$ cells/ml), harvested by centrifugation, and lysed in co-IP buffer (20 mM HEPES-KOH, pH 7.9, 200 mM potassium acetate, 10% glycerol, 0.1% Nonidet P-40 substitute (Sigma-Aldrich), 1 mM DTT, 1× protease inhibitors (0.1 mM PMSF, 1 mM benzamidine HCl, 2.5 μg/ml aprotinin, 2.5 μg/ml leupeptin, 1 μg/ml pepstatin A)) using glass bead beating. Soluble protein was separated from insoluble material by centrifugation at 20,800 × *g* for 15 min. Protein concentrations were determined using a BSA standard curve with the Bio-Rad Protein Assay. 2 mg of soluble protein extract were incubated with 2.5 μg of anti-HA 12CA5 mAb and 50 ng/μl ethidium bromide in a total volume of 412 μl at 4 °C for 2 h. Immune complexes were captured with 10 μl of protein A-Sepharose beads (Life Technologies) for 30 min with mixing at 4 °C. Captured protein complexes were washed two times with 1 ml of ice-cold co-IP buffer and eluted with 2× lithium dodecyl sulfate NuPAGE Sample Buffer (Life Technologies) and heating at 75 °C for 10 min. Proteins for both steady-state immunoblotting and co-immunoprecipitations were separated via SDS-PAGE using 4–12% NuPAGE Bis-Tris gradient gels (Life Technologies) run with 1× MOPS running buffer and electrotransferred to PVDF membranes using a wet transfer system. Polyclonal anti-Taf and anti-TBP antibodies were used

as described previously (60, 70). Anti-actin (mAb8224) and anti-HA HRP conjugate (3F10) antibodies were procured from Abcam and Roche Applied Science, respectively. Goat anti-rabbit (Fc) HRP conjugate and horse anti-mouse IgG HRP conjugate were procured from Thermo Fisher and Cell Signaling Technology, respectively. Protein signal was detected using Amersham Biosciences ECL Western blotting detection reagent (GE Healthcare) and exposed to Blue Basic double emulsion autoradiography film (GeneMate). For immunoblotting loading controls, the blot was stained with Ponceau S (0.5% (w/v) Ponceau-S in 1% (v/v) glacial acetic acid) following the electrotransfer and destained with H_2O prior to imaging.

Protein Overexpression and Purification—All His_6-tagged proteins were expressed from pET28a (Novagen). All His_6-GST-tagged proteins were plasmid-generated from pBG101 in Rosetta2 (DE3) *E. coli*. His_6-Taf14 and Taf2 fragments were N-terminally tagged with MGSS**HHHHHH**SSGLVPAGSHMAS (bold indicates the hexahistidine tag). *E. coli* expression strains were grown at 37 °C with shaking at 250 rpm to an optical density at 600 nm (OD_{600}) of 0.6–0.9, shifted to 30 °C, and induced for 4 h with 1 mM isopropyl β-D-1 thiogalactopyranoside. His_6-Taf14, His_6-GST, His_6-GST-Taf14(1–244), His_6-GST-Taf14(1–123), and His_6-GST-Taf14(124–244) were purified in the following manner. 4 g of *E. coli* pellet were lysed in 40 ml of *E. coli* lysis buffer (20 mM Tris-HCl, pH 7.9, 200 mM NaCl, 20 mM imidazole, 0.1% Triton X-100, 10% glycerol, 1 mM DTT, 1× protease inhibitors) in the presence of approximately 100 μg/ml lysozyme. Lysates were sonicated, and insoluble material was pelleted by spinning at 27,000 × *g* in a Sorvall RC 5C Plus centrifuge with an SS-34 rotor for 15 min. Soluble lysate was then bound in batch to 2 ml of Ni^{2+}-NTA-agarose (Qiagen) for 2 h at 4 °C with mixing. Ni^{2+}-NTA-agarose and bound proteins were transferred to disposable 20-ml chromatography columns (Bio-Rad) and washed in column format with >10 column volumes of *E. coli* lysis buffer. Proteins were eluted with elution buffer (lysis buffer without chicken egg white lysozyme but with 200 mM imidazole), and peak fractions were collected. His_6-Taf2 fragments were purified as described above with the following modifications for denaturing purification. Approximately 200 mg of *E. coli* pellet were lysed in 6 ml of denaturing lysis buffer (20 mM Tris-HCl, pH 7.9, 1× PBS, 6 M guanidinium HCl, 10 mM imidazole). Denatured cell extract was mixed with 200 μl of Ni^{2+}-NTA-agarose for 2 h at 20 °C. Ni^{2+}-NTA-agarose and bound proteins were washed with >10 column volumes of freshly made denaturing wash buffer (20 mM Tris-HCl, pH 7.9, 1× PBS, 7 M urea, 10 mM imidazole). His_6-Taf2 fragments were eluted with freshly made denaturing elution buffer (denaturing wash buffer except 200 mM imidazole). For all purified proteins, protein concentration was determined via in-gel quantitation using a BSA standard curve.

Purification of MBP-Taf2 from S. cerevisiae—MBP-3C cleavage site (MBP-3C) was derived from pLM302, a derivative of pET27 (Novagen) engineered to contain MBP (derived from pMAL (New England Biolabs)) followed by the PreScission protease cleavage site LEVLFQ↓GP and a multiple cloning site. MBP-3C and Taf2 or Taf2-ΔC fragments were sequentially cloned in p425GAL1 (84). An MBP-3C-only plasmid was also generated. MBP-3C, MBP-Taf2, and MBP-Taf2-ΔC expression plasmids were transformed in BY4741. Leu^+ colonies were grown at 30 °C with shaking at 250 rpm in SC −Leu with 1% (w/v) raffinose as the sole carbon source until the cultures reached a cell density of approximately 1.8×10^7 cells/ml. Solid galactose was added to the culture to reach a concentration of 2% (w/v), and the cells were allowed to grow for 3 h at 30 °C. Cells were harvested by centrifugation and stored at −80 °C until purification. For purification, all manipulations were performed at 4 °C or on ice unless specified. Typically, 30 g of yeast cell pellet were lysed in 30 ml of Taf2 purification buffer (20 mM HEPES-KOH, 500 mM potassium acetate, 0.5% Nonidet P-40 substitute, 10% glycerol, 2 mM DTT, and 2× protease inhibitors) using glass bead lysis. Lysate was then centrifuged at 27,000 × *g* in a Sorvall RC 5C Plus centrifuge with an SS-34 rotor for 15 min, and soluble cell extract was mixed with 5 ml of DE-52 resin equilibrated in Taf2 purification buffer for 10 min with mixing at 20 °C. DE-52 flow-through was then diluted with 20 mM HEPES-KOH, pH 7.9, 10% glycerol, 1 mM DTT, 1× protease inhibitors to reduce the potassium acetate and the Nonidet P-40 substitute concentration to 200 mM and 0.2%, respectively, and bound to 5 ml of amylose resin (New England Biolabs) in batch with mixing for 2 h. The amylose resin-bound proteins were transferred to a disposable chromatography column and washed with >10 column volumes amylose wash buffer (20 mM HEPES-KOH, pH 7.9, 200 mM potassium acetate, 0.1% Nonidet P-40 substitute, 10% glycerol, 1 mM DTT, 1× protease inhibitors). MBP-3C, MBP-Taf2, and MBP-Taf2-ΔC were eluted with wash buffer + 10 mM maltose, and peak fractions were collected. Alternatively, Taf2 was eluted with laboratory-generated 3C protease at 100 ng/ml concentration at 4 °C for 16 h. MBP-3C was subsequently dialyzed extensively against dialysis buffer (20 mM HEPES-KOH, 100 mM potassium acetate, 10% glycerol, 1 mM DTT, 1× protease inhibitors). MBP-Taf2, MBP-Taf2-ΔC, or free Taf2 was further purified using a Mono Q column (GE Healthcare). Peak eluate fractions from the amylose resin purification were loaded onto Mono Q with BA200 (BA = 20 mM HEPES-KOH, pH 7.9, 10% glycerol, 1 mM DTT, 1× protease inhibitors with variable concentrations of potassium acetate; *e.g.* BA200 contains 200 mM potassium acetate). Proteins were eluted with a linear gradient of BA200 to BA1500. Peak MBP-Taf2, MBP-Taf2-ΔC, and Taf2 fractions eluted at approximately BA1200. Peak fractions were pooled and dialyzed extensively against dialysis buffer.

Taf2/Taf14 Co-expression Solubilization Analyses—For Taf2 and Taf14 co-expression, a bicistronic expression plasmid was generated by cloning in order either full-length Taf14 or Taf14(164–244), an internal ribosome binding site sequence (88), and Taf2 C-terminal fragments (aa 1301–1407) into pET28a. Taf2 fragments contained a C-terminal KLAAALE**HHHHHH**(stop) tag. Taf2/Taf14 co-expression solubilization assays were performed by growing 6 ml of *E. coli* expression strains at 37 °C with shaking at 250 rpm to an OD_{600} of 0.6–0.9, shifted to 30 °C, and induced for 2 h with 1 mM isopropyl β-D-1 thiogalactopyranoside. One-sixth of the cell pellet was lysed in *E. coli* denaturing wash buffer for total cellular protein. The remaining cell pellet was lysed in 1 ml of *E. coli* lysis buffer with lysozyme as described above. Soluble protein was mixed with 7.5 μl of Q Sepharose to remove nucleic acids for 30 min at 4 °C.

The flow-through was mixed with 20 μl of Ni^{2+}-NTA-agarose for 2 h at 4 °C. Bound proteins were washed two times with 500 μl of *E. coli* lysis buffer and eluted with 200 μl of *E. coli* elution buffer. Total cellular protein and purified Taf2-Taf14 complexes were separated via SDS-PAGE as described above except running with 1× MES buffer (Life Technologies) to separate smaller protein species. The proteins were visualized using Coomassie Brilliant Blue.

TFIID Purification—HA_{x1}-Taf1 TFIID and HA_{x1}-Taf1 Taf2-ΔC TFIID were purified essentially as described (8, 46) with the following modifications. Extracts prepared according to Woontner *et al.* (89) were dialyzed against 20 mM HEPES-KOH, pH 7.9, 50 mM potassium acetate, 20% glycerol, 5 mM DTT, 1× protease inhibitor mixture until the dialysate reached a conductivity equivalent to BA300. Dialyzed extract derived from a maximum of 300 g of yeast cell pellet was chromatographed over a 200-ml Bio-Rex70 100–200-mesh column. For immunopurification, 10% Surfact-Amps Nonidet P-40 was added to the Bio-Rex70 1 M fraction to a final concentration of 0.2%. The Bio-Rex70 1 M fraction was subsequently diluted 1:2 in BA0, ethidium bromide was added to a final concentration of 50 μg/ml, and the fraction was subjected to anti-HA affinity chromatography with 10 mg of anti-HA 12CA5 mAb covalently coupled to 2.5 ml of protein A-Sepharose beads (Life Technologies) at 4 °C for 16 h with mixing. Bound proteins were transferred to a 10-ml disposable chromatography column, washed with >5 column volumes of BA300 with 0.1% Surfact-Amps Nonidet P-40, >5 column volumes of BA300 with 0.01% Surfact-Amps Nonidet P-40, and >5 column volumes of BA300 with 0.001% Surfact-Amps Nonidet P-40. TFIID was eluted from the column two times with 2.5 ml of elution buffer (BA300 with 0.001% Surfact-Amps Nonidet P-40 plus 2 mg/ml HA_{x1} peptide) for 30 min at 20 °C with mixing. The HA_{x1} peptide eluate was immediately subjected to ion exchange chromatography on a 1.2-ml UnoS column (Bio-Rad). Following binding of the HA_{x1} peptide eluate, the UnoS column was washed with >5 column volumes of BA300 and then subjected to a linear gradient of BA300 to BA1000. TFIID elutes at approximately BA650.

Taf1-TAP TFIID was purified according to a modified tandem affinity purification protocol. 1 kg of YLSTAF1 (41) pellet was lysed in 500 ml of 3× TAP buffer (0.45 M Tris acetate, pH 7.8, 0.15 M potassium acetate, 60% glycerol, 3 mM DTT, 3 mM EDTA, 3× protease inhibitors) using glass bead lysis. Then the salt concentration of the lysate was adjusted with 5 M potassium acetate to the conductivity equivalent of 300 mM potassium acetate and centrifuged at 205,000 × *g* in a Beckman Optima LE-80K ultracentrifuge with a Ti-45 rotor for 90 min. The supernatant was collected, avoiding the turbid material at the bottom of the centrifugation tube, and then bound to 100 ml of IgG-Sepharose (GE Healthcare)/liter of protein extract in batch at 4 °C for 2 h with mixing. Following binding, the IgG-Sepharose and bound protein were washed extensively in IgG-Sepharose binding buffer (20 mM Tris acetate, pH 7.8, 300 mM potassium acetate, 10% glycerol, 0.5 mM EDTA, 1 mM DTT, 1× protease inhibitors). TFIID was eluted from the IgG-Sepharose in 100 ml of IgG-Sepharose binding buffer plus tobacco etch virus protease at 250 ng/ml for 2 h at 4 °C. Following tobacco etch virus protease elution from IgG-Sepharose, the eluate was immediately subjected to ion exchange chromatography on a 1.2-ml UnoS column as described above. TFIID elutes at approximately BA650.

Far-Western Blotting—0.5 pmol of Taf1-TAP TFIID, 5 pmol of purified MBP-3C, 1 pmol of MBP-Taf2, and between 1 and 5pmol of Taf2 truncation variants were subjected to Far-Western blotting analysis with a His_6-Taf14 overlay essentially as described (28) with the following modifications. For all analyses, proteins samples were subjected to SDS-PAGE in triplicate: one gel for SYPRO Ruby gel staining, one mock overlay control, and one His_6-Taf14 binding assay. During the blotting process, all binding steps and washes were performed in renaturation buffer (20 mM HEPES-KOH, pH 7.6, 75 mM potassium chloride, 2.5 mM magnesium chloride, 0.25 mM EDTA, 0.05% Triton X-100 with 1 mM DTT freshly added). The overlay was performed with 7 nM His_6-Taf14 with 1% BSA as a nonspecific competitor or with just the BSA competitor for the mock control. Bound His_6-Taf14 was detected using a standard immunoblotting protocol (primary antibody, antigen affinity-purified anti-Taf14 polyclonal rabbit IgG at a concentration of 0.1 ng/ml; secondary antibody, goat anti-rabbit Fc-HRP used according to the manufacturer's instructions). Prior to treatment with ECL reagent and exposure to film, the blots were washed once with Tris-buffered saline (25 mM Tris-HCl, pH 7.5, 150 mM NaCl).

GST Pulldown Assays—Typically, binding reactions were performed in a total volume of 200 μl in the following reaction buffer: 20 mM HEPES-KOH, pH 7.9, 300 mM potassium acetate, 10% glycerol, 1 mM DTT, 0.1% Nonidet P-40 substitute, 0.1 mg/ml BSA. MBP-Taf2 and MBP-Taf2-ΔC GST pulldowns were performed twice, either with 2 pmol of His_6-GST-Taf14 or 5 pmol of His_6-GST-Taf14 and twice that amount with His_6-GST-only pulldowns. Between 1 and 32 pmol of MBP-Taf2 or MBP-Taf2-ΔC were used in the binding assays. For Taf2 binding assays, 16 pmol of His_6-GST, 8 pmol of His_6-GST-Taf14, 12 pmol of His_6-GST-Taf14(1–123), and 12 pmol of His_6-GST-Taf14(124–244) were used. These proteins were mixed either with no Taf2 or with between 0.78 and 6.25 pmol of Taf2. Binding reactions were allowed to proceed at 20 °C for 1 h followed by 30-min capture at 20 °C with 10 μl of a 1:1 slurry of glutathione-agarose Fast Flow (GE Healthcare) equilibrated in reaction buffer. Glutathione-agarose-bound complexes were pelleted by centrifugation, and the supernatant was discarded. The pellet was washed with 500 μl of binding buffer without BSA and pelleted again, and the wash buffer was discarded. Bound proteins were eluted with 2× lithium dodecyl sulfate sample buffer with 100 mM DTT, heating at 75 °C for 10 min. Proteins were separated with 4–12% NuPAGE Bis-Tris gradient gels run with 1× MOPS running buffer and stained with SYPRO Ruby according to the manufacturer's instructions. Proteins were imaged with a PharosFX scanner (Bio-Rad).

qRT-PCR—For all RNA analyses, JFTAF2del was used as the parent strain. For temperature shift experiments, this strain was co-transformed with p415ADH-*HA_{x3}NLS-TAF2* or p415ADH-*HA_{x3}NLS-taf2-ts7* and either p413GPD or p413GPD-*$FLAG_{x2}$NLS-TAF14*. Leu^+His^+ colonies were sub-

jected to plasmid shuffle on SC −His,−Leu + 5-FOA. For each co-transformed shuffled strain, two independent colonies were grown in SC −His,−Leu at 25 °C until they reached a cell density of ~1.2×10^7 cells/ml, then abruptly shifted to 37 °C by adding an equal volume of 50 °C heated SC −His,−Leu, and then grown at 37 °C for 2 h. Cells were harvested by centrifugation, and pellets were stored at −80 °C. For steady-state RNA experiments, JFTAF2del was transformed with either p415ADH-*HA*$_{x3}$*NLS-TAF2* or p415ADH-*HA*$_{x3}$*NLS-taf2-ΔC*. Leu$^+$ colonies were subjected to plasmid shuffle by growth on SC −Leu + 5-FOA. For each shuffled strain, four independent colonies were grown in YPD until the cells reached ~2.4×10^7 cells/ml and harvested by filtration.

For all samples, RNA was extracted using hot acidic phenol as described (90). Reverse transcription was performed with 1 μg of total RNA using Superscript III according to the manufacturer's instructions. cDNA was generated using oligo(dT)$_{16}$ and 1 pmol each of gene-specific reverse primers for U3, RDN58, and SNR6. The primer sequences used in these analyses are as follows: U3-F, CAAAAGAGCCACTGAATCCAACTTGG; U3-R, GTACCCACCCATAGAGCCCTATCCCTTC; RDN58-F, AACGGATCTCTTGGTTCTCG; RDN58-R, GTGCGTTCAAAGATTCGATG; SNR6-F, CGAAGTAACCCTTCGTGGAC; SNR6-R, TCATCCTTATGCAGGGGAAC (54); RPS3-F, TACGGTGTCGTCAGATACG; RPS3-R, GACCAGAGTGAATCAAGAAACC; RPS5-F, GGATGCTTCTTTGGTTGACTAC; RPS5-R, GGACATTGAGCCTTTCTGAATCTC; RPS8A-F, AAAGATCCGCTACCGGTGCCAAG; RPS8A-R, TCTTGGAGATACCTTCAGAAGCCC; RPS9B-F, CGGTTTGAAGAACAAGAGA; RPS9B-R, GCATTACCTTCGAACAATC; PGK1-F, TGCTGCTTTGCCAACCATC; PGK1-R, GTGACATCCTTACCCAACAATG; PYK1-F, CCAACCTCCACCACCGAAAC; PYK1-R, GGGCTTCAACATCATCAGTCCA (28).

Quantitative PCR was performed using SYBR Green Supermix (Bio-Rad) according to the manufacturer's instructions. Samples were quantified using the relative standard curve method, normalized to U3, and expressed as a percentage of the average of the *HA-TAF2* strain. The standard curve was generated by mixing equal amounts of RNA from each of the samples tested prior to reverse transcription. This RNA mixture was used both as the standard curve and as the no-RT control. Three values were used for each standard curve based on the dilution of the cDNA. For example, if a dilution of 1:50 was used to measure the experimental cDNA samples, then a standard curve of 1:5, 1:50, and 1:500 was used. The no-RT reactions displayed either no observable signal or required an additional 10 C_t values above the +RT samples to achieve measureable signal. Thus, we concluded that contaminating genomic DNA was negligible in the samples. The dilutions used for each gene are as follows: 1:50 for *RPS3*, *RPS5*, *RPS8A*, *RPS9B*, and *SNR6*; 1:1000 for *PGK1*, *PYK1*, and *U3*; and 1:20,000 for *RDN58*. All qPCRs were performed in triplicate. Individual technical replicates were only discarded as outliers if C_t values were different from the other technical replicates by greater than a full C_t value and the amplification trace displayed apparent aberrations in amplification efficiency.

Author Contributions—J. T. F. and P. A. W. conceived the project. J. T. F. conducted all of the experiments, analyzed the results, and wrote the paper. P. A. W. advised on experimental approaches and edited the manuscript.

Acknowledgments—We thank our colleagues Amanda Johnson and Dr. Chirie Sumanasekera for ideas and support during the execution of this project. We also thank Dr. Katherine Hutchinson-Feigerle for helping plate the thousands of transformation reactions required to complete this study.

References

1. Hahn, S., and Young, E. T. (2011) Transcriptional regulation in *Saccharomyces cerevisiae*: transcription factor regulation and function, mechanisms of initiation, and roles of activators and coactivators. *Genetics* **189,** 705–736
2. Thomas, M. C., and Chiang, C.-M. (2006) The general transcription machinery and general cofactors. *Crit. Rev. Biochem. Mol. Biol.* **41,** 105–178
3. Li, X. Y., Bhaumik, S. R., and Green, M. R. (2000) Distinct classes of yeast promoters revealed by differential TAF recruitment. *Science* **288,** 1242–1244
4. Shen, W.-C., Bhaumik, S. R., Causton, H. C., Simon, I., Zhu, X., Jennings, E. G., Wang, T.-H., Young, R. A., and Green, M. R. (2003) Systematic analysis of essential yeast TAFs in genome-wide transcription and preinitiation complex assembly. *EMBO J.* **22,** 3395–3402
5. Huisinga, K. L., and Pugh, B. F. (2004) A genome-wide housekeeping role for TFIID and a highly regulated stress-related role for SAGA in *Saccharomyces cerevisiae*. *Mol. Cell* **13,** 573–585
6. Basehoar, A. D., Zanton, S. J., and Pugh, B. F. (2004) Identification and distinct regulation of yeast TATA box-containing genes. *Cell* **116,** 699–709
7. Rhee, H. S., and Pugh, B. F. (2012) Genome-wide structure and organization of eukaryotic pre-initiation complexes. *Nature* **483,** 295–301
8. Sanders, S. L., Garbett, K. A., and Weil, P. A. (2002) Molecular characterization of *Saccharomyces cerevisiae* TFIID. *Mol. Cell. Biol.* **22,** 6000–6013
9. Tora, L. (2002) A unified nomenclature for TATA box binding protein (TBP)-associated factors (TAFs) involved in RNA polymerase II transcription. *Genes Dev.* **16,** 673–675
10. Verrijzer, C. P., Yokomori, K., Chen, J. L., and Tjian, R. (1994) *Drosophila* TAF$_{II}$150: similarity to yeast gene *TSM-1* and specific binding to core promoter DNA. *Science* **264,** 933–941
11. Burke, T. W., and Kadonaga, J. T. (1997) The downstream core promoter element, DPE, is conserved from *Drosophila* to humans and is recognized by TAF$_{II}$60 of *Drosophila*. *Genes Dev.* **11,** 3020–3031
12. Chalkley, G. E., and Verrijzer, C. P. (1999) DNA binding site selection by RNA polymerase II TAFs: a TAF$_{II}$250-TAF$_{II}$150 complex recognizes the initiator. *EMBO J.* **18,** 4835–4845
13. Albright, S. R., and Tjian, R. (2000) TAFs revisited: more data reveal new twists and confirm old ideas. *Gene* **242,** 1–13
14. Lim, C. Y., Santoso, B., Boulay, T., Dong, E., Ohler, U., and Kadonaga, J. T. (2004) The MTE, a new core promoter element for transcription by RNA polymerase II. *Genes Dev.* **18,** 1606–1617
15. Shao, H., Revach, M., Moshonov, S., Tzuman, Y., Gazit, K., Albeck, S., Unger, T., and Dikstein, R. (2005) Core promoter binding by histone-like TAF complexes. *Mol. Cell. Biol.* **25,** 206–219
16. Gazit, K., Moshonov, S., Elfakess, R., Sharon, M., Mengus, G., Davidson, I., and Dikstein, R. (2009) TAF4/4b·TAF12 displays a unique mode of DNA binding and is required for core promoter function of a subset of genes. *J. Biol. Chem.* **284,** 26286–26296
17. Cianfrocco, M. A., Kassavetis, G. A., Grob, P., Fang, J., Juven-Gershon, T., Kadonaga, J. T., and Nogales, E. (2013) Human TFIID binds to core promoter DNA in a reorganized structural state. *Cell* **152,** 120–131
18. Kaufmann, J., Ahrens, K., Koop, R., Smale, S. T., and Müller, R. (1998) CIF150, a human cofactor for transcription factor IID-dependent initiator function. *Mol. Cell. Biol.* **18,** 233–239

19. Kaufmann, J., Verrijzer, C. P., Shao, J., and Smale, S. T. (1996) CIF, an essential cofactor for TFIID-dependent initiator function. *Genes Dev.* **10,** 873–886
20. Mizzen, C. A., Yang, X. J., Kokubo, T., Brownell, J. E., Bannister, A. J., Owen-Hughes, T., Workman, J., Wang, L., Berger, S. L., Kouzarides, T., Nakatani, Y., and Allis, C. D. (1996) The $TAF_{II}250$ subunit of TFIID has histone acetyltransferase activity. *Cell* **87,** 1261–1270
21. Jacobson, R. H., Ladurner, A. G., King, D. S., and Tjian, R. (2000) Structure and function of a human $TAF_{II}250$ double bromodomain module. *Science* **288,** 1422–1425
22. Vermeulen, M., Mulder, K. W., Denissov, S., Pijnappel, W. W., van Schaik, F. M., Varier, R. A., Baltissen, M. P., Stunnenberg, H. G., Mann, M., and Timmers, H. T. (2007) Selective anchoring of TFIID to nucleosomes by trimethylation of histone H3 lysine 4. *Cell* **131,** 58–69
23. Shanle, E. K., Andrews, F. H., Meriesh, H., McDaniel, S. L., Dronamraju, R., DiFiore, J. V., Jha, D., Wozniak, G. G., Bridgers, J. B., Kerschner, J. L., Krajewski, K., Martín, G. M., Morrison, A. J., Kutateladze, T. G., and Strahl, B. D. (2015) Association of Taf14 with acetylated histone H3 directs gene transcription and the DNA damage response. *Genes Dev.* **29,** 1795–1800
24. Andrews, F. H., Shinsky, S. A., Shanle, E. K., Bridgers, J. B., Gest, A., Tsun, I. K., Krajewski, K., Shi, X., Strahl, B. D., and Kutateladze, T. G. (2016) The Taf14 YEATS domain is a reader of histone crotonylation. *Nat. Chem. Biol.* **12,** 396–398
25. van Nuland, R., Schram, A. W., van Schaik, F. M., Jansen, P. W., Vermeulen, M., and Marc Timmers, H. T. (2013) Multivalent engagement of TFIID to nucleosomes. *PLoS One* **8,** e73495
26. Tanese, N., Pugh, B. F., and Tjian, R. (1991) Coactivators for a proline-rich activator purified from the multisubunit human TFIID complex. *Genes Dev.* **5,** 2212–2224
27. Dynlacht, B. D., Hoey, T., and Tjian, R. (1991) Isolation of coactivators associated with the TATA-binding protein that mediate transcriptional activation. *Cell* **66,** 563–576
28. Garbett, K. A., Tripathi, M. K., Cencki, B., Layer, J. H., and Weil, P. A. (2007) Yeast TFIID serves as a coactivator for Rap1p by direct protein-protein interaction. *Mol. Cell. Biol.* **27,** 297–311
29. Liu, W.-L., Coleman, R. A., Ma, E., Grob, P., Yang, J. L., Zhang, Y., Dailey, G., Nogales, E., and Tjian, R. (2009) Structures of three distinct activator-TFIID complexes. *Genes Dev.* **23,** 1510–1521
30. Kraemer, S. M., Ranallo, R. T., Ogg, R. C., and Stargell, L. A. (2001) TFIIA interacts with TFIID via association with TATA-binding protein and TAF40. *Mol. Cell. Biol.* **21,** 1737–1746
31. Robinson, M. M., Yatherajam, G., Ranallo, R. T., Bric, A., Paule, M. R., and Stargell, L. A. (2005) Mapping and functional characterization of the TAF11 interaction with TFIIA. *Mol. Cell. Biol.* **25,** 945–957
32. Layer, J. H., and Weil, P. A. (2013) Direct TFIIA-TFIID protein contacts drive budding yeast ribosomal protein gene transcription. *J. Biol. Chem.* **288,** 23273–23294
33. Guermah, M., Tao, Y., and Roeder, R. G. (2001) Positive and negative TAF_{II} functions that suggest a dynamic TFIID structure and elicit synergy with traps in activator-induced transcription. *Mol. Cell. Biol.* **21,** 6882–6894
34. Olave, I., Reinberg, D., and Vales, L. D. (1998) The mammalian transcriptional repressor RBP (CBF1) targets TFIID and TFIIA to prevent activated transcription. *Genes Dev.* **12,** 1621–1637
35. Takahashi, H., Parmely, T. J., Sato, S., Tomomori-Sato, C., Banks, C. A., Kong, S. E., Szutorisz, H., Swanson, S. K., Martin-Brown, S., Washburn, M. P., Florens, L., Seidel, C. W., Lin, C., Smith, E. R., Shilatifard, A., Conaway, R. C., and Conaway, J. W. (2011) Human mediator subunit MED26 functions as a docking site for transcription elongation factors. *Cell* **146,** 92–104
36. Layer, J. H., Miller, S. G., and Weil, P. A. (2010) Direct transactivator-transcription factor IID (TFIID) contacts drive yeast ribosomal protein gene transcription. *J. Biol. Chem.* **285,** 15489–15499
37. Lauberth, S. M., Nakayama, T., Wu, X., Ferris, A. L., Tang, Z., Hughes, S. H., and Roeder, R. G. (2013) H3K4me3 interactions with TAF3 regulate preinitiation complex assembly and selective gene activation. *Cell.* **152,** 1021–1036
38. Brand, M., Leurent, C., Mallouh, V., Tora, L., and Schultz, P. (1999) Three-dimensional structures of the TAF_{II}-containing complexes TFIID and TFTC. *Science* **286,** 2151–2153
39. Papai, G., Weil, P. A., and Schultz, P. (2011) New insights into the function of transcription factor TFIID from recent structural studies. *Curr. Opin. Genet. Dev.* **21,** 219–224
40. Leurent, C., Sanders, S., Ruhlmann, C., Mallouh, V., Weil, P. A., Kirschner, D. B., Tora, L., and Schultz, P. (2002) Mapping histone fold TAFs within yeast TFIID. *EMBO J.* **21,** 3424–3433
41. Papai, G., Tripathi, M. K., Ruhlmann, C., Werten, S., Crucifix, C., Weil, P. A., and Schultz, P. (2009) Mapping the initiator binding Taf2 subunit in the structure of hydrated yeast TFIID. *Structure* **17,** 363–373
42. Leurent, C., Sanders, S. L., Demény, M. A., Garbett, K. A., Ruhlmann, C., Weil, P. A., Tora, L., and Schultz, P. (2004) Mapping key functional sites within yeast TFIID. *EMBO J.* **23,** 719–727
43. Bieniossek, C., Papai, G., Schaffitzel, C., Garzoni, F., Chaillet, M., Scheer, E., Papadopoulos, P., Tora, L., Schultz, P., and Berger, I. (2013) The architecture of human general transcription factor TFIID core complex. *Nature* **493,** 699–702
44. Trowitzsch, S., Viola, C., Scheer, E., Conic, S., Chavant, V., Fournier, M., Papai, G., Ebong, I.-O., Schaffitzel, C., Zou, J., Haffke, M., Rappsilber, J., Robinson, C. V., Schultz, P., Tora, L., and Berger, I. (2015) Cytoplasmic TAF2-TAF8-TAF10 complex provides evidence for nuclear holo-TFIID assembly from preformed submodules. *Nat. Commun.* **6,** 6011
45. Reese, J. C., Apone, L., Walker, S. S., Griffin, L. A., and Green, M. R. (1994) Yeast $TAF_{II}S$ in a multisubunit complex required for activated transcription. *Nature* **371,** 523–527
46. Poon, D., Bai, Y., Campbell, A. M., Bjorklund, S., Kim, Y. J., Zhou, S., Kornberg, R. D., and Weil, P. A. (1995) Identification and characterization of a TFIID-like multiprotein complex from *Saccharomyces cerevisiae*. *Proc. Natl. Acad. Sci. U.S.A.* **92,** 8224–8228
47. Gangloff, Y. G., Sanders, S. L., Romier, C., Kirschner, D., Weil, P. A., Tora, L., and Davidson, I. (2001) Histone folds mediate selective heterodimerization of yeast $TAF_{II}25$ with TFIID components $yTAF_{II}47$ and $yTAF_{II}65$ and with SAGA component ySPT7. *Mol. Cell. Biol.* **21,** 1841–1853
48. Matangkasombut, O., Buratowski, R. M., Swilling, N. W., and Buratowski, S. (2000) Bromodomain factor 1 corresponds to a missing piece of yeast TFIID. *Genes Dev.* **14,** 951–962
49. Ladurner, A. G., Inouye, C., Jain, R., and Tjian, R. (2003) Bromodomains mediate an acetyl-histone encoded antisilencing function at heterochromatin boundaries. *Mol. Cell* **11,** 365–376
50. Schulze, J. M., Wang, A. Y., and Kobor, M. S. (2009) YEATS domain proteins: a diverse family with many links to chromatin modification and transcription. *Biochem. Cell Biol.* **87,** 65–75
51. Welch, M. D., and Drubin, D. G. (1994) A nuclear protein with sequence similarity to proteins implicated in human acute leukemias is important for cellular morphogenesis and actin cytoskeletal function in *Saccharomyces cerevisiae*. *Mol. Biol. Cell.* **5,** 617–632
52. Cairns, B. R., Henry, N. L., and Kornberg, R. D. (1996) TFG/TAF30/ANC1, a component of the yeast SWI/SNF complex that is similar to the leukemogenic proteins ENL and AF-9. *Mol. Cell. Biol.* **16,** 3308–3316
53. Lin, C., Smith, E. R., Takahashi, H., Lai, K. C., Martin-Brown, S., Florens, L., Washburn, M. P., Conaway, J. W., Conaway, R. C., and Shilatifard, A. (2010) AFF4, a component of the ELL/P-TEFb elongation complex and a shared subunit of MLL chimeras, can link transcription elongation to leukemia. *Mol. Cell* **37,** 429–437
54. Bonnet, J., Wang, C.-Y., Baptista, T., Vincent, S. D., Hsiao, W.-C., Stierle, M., Kao, C.-F., Tora, L., and Devys, D. (2014) The SAGA coactivator complex acts on the whole transcribed genome and is required for RNA polymerase II transcription. *Genes Dev.* **28,** 1999–2012
55. Li, Y., Sabari, B. R., Panchenko, T., Wen, H., Zhao, D., Guan, H., Wan, L., Huang, H., Tang, Z., Zhao, Y., Roeder, R. G., Shi, X., Allis, C. D., and Li, H. (2016) Molecular coupling of histone crotonylation and active transcription by AF9 YEATS domain. *Mol. Cell* **62,** 181–193
56. Oelgeschläger, T., Chiang, C. M., and Roeder, R. G. (1996) Topology and reorganization of a human TFIID-promoter complex. *Nature* **382,** 735–738

57. Papai, G., Tripathi, M. K., Ruhlmann, C., Layer, J. H., Weil, P. A., and Schultz, P. (2010) TFIIA and the transactivator Rap1 cooperate to commit TFIID for transcription initiation. *Nature* **465,** 956–960
58. Henry, N. L., Campbell, A. M., Feaver, W. J., Poon, D., Weil, P. A., and Kornberg, R. D. (1994) TFIIF-TAF-RNA polymerase II connection. *Genes Dev.* **8,** 2868–2878
59. Kabani, M., Michot, K., Boschiero, C., and Werner, M. (2005) Anc1 interacts with the catalytic subunits of the general transcription factors TFIID and TFIIF, the chromatin remodeling complexes RSC and INO80, and the histone acetyltransferase complex NuA3. *Biochem. Biophys. Res. Commun.* **332,** 398–403
60. Sanders, S. L., Jennings, J., Canutescu, A., Link, A. J., and Weil, P. A. (2002) Proteomics of the eukaryotic transcription machinery: identification of proteins associated with components of yeast TFIID by multidimensional mass spectrometry. *Mol. Cell. Biol.* **22,** 4723–4738
61. Ray, B. L., White, C. I., and Haber, J. E. (1991) The *TSM1* gene of *Saccharomyces cerevisiae* overlaps the MAT locus. *Curr. Genet.* **20,** 25–31
62. Klebanow, E. R., Poon, D., Zhou, S., and Weil, P. A. (1996) Isolation and characterization of *TAF25*, an essential yeast gene that encodes an RNA polymerase II-specific TATA-binding protein-associated factor. *J. Biol. Chem.* **271,** 13706–13715
63. Klebanow, E. R., Poon, D., Zhou, S., and Weil, P. A. (1997) Cloning and characterization of an essential *Saccharomyces cerevisiae* gene, *TAF40*, which encodes yTAF$_{II}$40, an RNA polymerase II-specific TATA-binding protein-associated factor. *J. Biol. Chem.* **272,** 9436–9442
64. Moqtaderi, Z., Yale, J. D., Struhl, K., and Buratowski, S. (1996) Yeast homologues of higher eukaryotic TFIID subunits. *Proc. Natl. Acad. Sci. U.S.A.* **93,** 14654–14658
65. Sanders, S. L., and Weil, P. A. (2000) Identification of two novel TAF subunits of the yeast *Saccharomyces cerevisiae* TFIID complex. *J. Biol. Chem.* **275,** 13895–13900
66. Zhang, Z., Boskovic, Z., Hussain, M. M., Hu, W., Inouye, C., Kim, H.-J., Abole, A. K., Doud, M. K., Lewis, T. A., Koehler, A. N., Schreiber, S. L., and Tjian, R. (2015) Chemical perturbation of an intrinsically disordered region of TFIID distinguishes two modes of transcription initiation. *eLife* **4,** e07777
67. Yakovchuk, P., Gilman, B., Goodrich, J. A., and Kugel, J. F. (2010) RNA polymerase II and TAFs undergo a slow isomerization after the polymerase is recruited to promoter-bound TFIID. *J. Mol. Biol.* **397,** 57–68
68. Louder, R. K., He, Y., López-Blanco, J. R., Fang, J., Chacón, P., and Nogales, E. (2016) Structure of promoter-bound TFIID and model of human pre-initiation complex assembly. *Nature* **531,** 604–609
69. Poon, D., Schroeder, S., Wang, C. K., Yamamoto, T., Horikoshi, M., Roeder, R. G., and Weil, P. A. (1991) The conserved carboxy-terminal domain of *Saccharomyces cerevisiae* TFIID is sufficient to support normal cell growth. *Mol. Cell. Biol.* **11,** 4809–4821
70. Singh, M. V., Bland, C. E., and Weil, P. A. (2004) Molecular and genetic characterization of a Taf1p domain essential for yeast TFIID assembly. *Mol. Cell. Biol.* **24,** 4929–4942
71. Bai, Y., Perez, G. M., Beechem, J. M., and Weil, P. A. (1997) Structure-function analysis of TAF130: identification and characterization of a high-affinity TATA-binding protein interaction domain in the N terminus of yeast TAF$_{II}$130. *Mol. Cell. Biol.* **17,** 3081–3093
72. Yang, J., and Zhang, Y. (2015) I-TASSER server: new development for protein structure and function predictions. *Nucleic Acids Res.* **43,** W174–W181
73. Plaschka, C., Hantsche, M., Dienemann, C., Burzinski, C., Plitzko, J., and Cramer, P. (2016) Transcription initiation complex structures elucidate DNA opening. *Nature* **533,** 353–358
74. Reiss, D. J., and Mobley, H. L. (2011) Determination of target sequence bound by PapX, repressor of bacterial motility, in *flhD* promoter using systematic evolution of ligands by exponential enrichment (SELEX) and high throughput sequencing. *J. Biol. Chem.* **286,** 44726–44738
75. Yoshikawa, K., Tanaka, T., Ida, Y., Furusawa, C., Hirasawa, T., and Shimizu, H. (2011) Comprehensive phenotypic analysis of single-gene deletion and overexpression strains of *Saccharomyces cerevisiae*. *Yeast* **28,** 349–361
76. Schulze, J. M., Kane, C. M., and Ruiz-Manzano, A. (2010) The YEATS domain of Taf14 in *Saccharomyces cerevisiae* has a negative impact on cell growth. *Mol. Genet. Genomics* **283,** 365–380
77. Knutson, B. A., and Hahn, S. (2011) Domains of Tra1 important for activator recruitment and transcription coactivator functions of SAGA and NuA4 complexes. *Mol. Cell. Biol.* **31,** 818–831
78. Dabrowski, S., and Kur, J. (1998) Cloning and expression in *Escherichia coli* of the recombinant His-tagged DNA polymerases from *Pyrococcus furiosus* and *Pyrococcus woesei*. *Protein Expr. Purif.* **14,** 131–138
79. Ho, S. N., Hunt, H. D., Horton, R. M., Pullen, J. K., and Pease, L. R. (1989) Site-directed mutagenesis by overlap extension using the polymerase chain reaction. *Gene* **77,** 51–59
80. Gietz, R. D., and Schiestl, R. H. (2007) High-efficiency yeast transformation using the LiAc/SS carrier DNA/PEG method. *Nat. Protoc.* **2,** 31–34
81. Boeke, J. D., Trueheart, J., Natsoulis, G., and Fink, G. R. (1987) 5-Fluoroorotic acid as a selective agent in yeast molecular genetics. *Methods Enzymol.* **154,** 164–175
82. Brachmann, C. B., Davies, A., Cost, G. J., Caputo, E., Li, J., Hieter, P., and Boeke, J. D. (1998) Designer deletion strains derived from *Saccharomyces cerevisiae* S288C: a useful set of strains and plasmids for PCR-mediated gene disruption and other applications. *Yeast* **14,** 115–132
83. Mumberg, D., Müller, R., and Funk, M. (1995) Yeast vectors for the controlled expression of heterologous proteins in different genetic backgrounds. *Gene* **156,** 119–122
84. Mumberg, D., Müller, R., and Funk, M. (1994) Regulatable promoters of *Saccharomyces cerevisiae*: comparison of transcriptional activity and their use for heterologous expression. *Nucleic Acids Res.* **22,** 5767–5768
85. Goldstein, A. L., and McCusker, J. H. (1999) Three new dominant drug resistance cassettes for gene disruption in *Saccharomyces cerevisiae*. *Yeast* **15,** 1541–1553
86. Poon, D., Campbell, A. M., Bai, Y., and Weil, P. A. (1994) Yeast Taf170 is encoded by MOT1 and exists in a TATA box-binding protein (TBP)-TBP-associated factor complex distinct from transcription factor IID. *J. Biol. Chem.* **269,** 23135–23140
87. Kushnirov, V. V. (2000) Rapid and reliable protein extraction from yeast. *Yeast* **16,** 857–860
88. Lutzmann, M., Kunze, R., Buerer, A., Aebi, U., and Hurt, E. (2002) Modular self-assembly of a Y-shaped multiprotein complex from seven nucleoporins. *EMBO J.* **21,** 387–397
89. Woontner, M., Wade, P. A., Bonner, J., and Jaehning, J. A. (1991) Transcriptional activation in an improved whole-cell extract from *Saccharomyces cerevisiae*. *Mol. Cell. Biol.* **11,** 4555–4560
90. Schmitt, M. E., Brown, T. A., and Trumpower, B. L. (1990) A rapid and simple method for preparation of RNA from *Saccharomyces cerevisiae*. *Nucleic Acids Res.* **18,** 3091–3092